Free Radical Biology and Medicine 207 (2023) 144–160

Contents lists available at ScienceDirect

Free Radical Biology and Medicine

journal homepage: www.elsevier.com/locate/freeradbiomed

Sex-specific metabolic adaptations in transgenic mice overexpressing cytochrome b_5 reductase-3

Luz Marina Sánchez-Mendoza [a], Carlos Pérez-Sánchez [a,b], Sandra Rodríguez-López [a], Chary López-Pedrera [b], Miguel Calvo-Rubio [c], Rafael de Cabo [c], María I. Burón [a], José A. González-Reyes [a], José M. Villalba [a,*]

[a] Departamento de Biología Celular, Fisiología e Inmunología, Universidad de Córdoba, Campus de Excelencia Internacional Agroalimentario, CeiA3, Córdoba, Spain
[b] Rheumatology Service, Reina Sofia Hospital/ Maimonides Institute for Research in Biomedicine of Cordoba (IMIBIC)/University of Cordoba, Cordoba, Spain
[c] Experimental Gerontology Section, Translational Gerontology Branch, National Institute on Aging, National Institutes of Health, Baltimore, MD, 21224, USA

ARTICLE INFO

Keywords:
CYB5R3
Mitochondria
Sexual dimorphism
Skeletal muscle

ABSTRACT

Cytochrome b_5 reductase 3 (CYB5R3) activates respiratory metabolism in cellular systems and exerts a pro-longevity action in transgenic mice overexpressing this enzyme, mimicking some of the beneficial effects of calorie restriction. The aim of our study was to investigate the role of sex on metabolic adaptations elicited by CYB5R3 overexpression, and how key markers related with mitochondrial function are modulated in skeletal muscle, one of the major contributors to resting energy expenditure. Young CYB5R3 transgenic mice did not exhibit the striking adaptations in carbon metabolism previously detected in older animals. CYB5R3 was efficiently overexpressed and targeted to mitochondria in skeletal muscle from transgenic mice regardless sex. Overexpression significantly elevated NADH in both sexes, although differences were not statistically significant for NAD^+, and increased the abundance of cytochrome *c* and the fission protein DRP-1 in females but not in males. Moreover, while mitochondrial biogenesis and function markers (as TFAM, NRF-1 and cleaved SIRT3) were markedly upregulated by CYB5R3 overexpression in females, a downregulation was observed in males. Ultrastructural changes were also highlighted, with an increase in the number of mitochondria per surface unit, and in the size of intermyofibrillar mitochondria in transgenic females compared with their wild-type controls. Our results support that CYB5R3 overexpression upregulates markers consistent with enhanced mitochondrial biogenesis and function, and increases mitochondrial abundance in skeletal muscle, producing most of these potentially beneficial actions in females.

1. Introduction

NADH-cytochrome b_5 reductases (CYB5R, EC 1.6.2.2) comprises a family of 4 flavoproteins which oxidize NADH to NAD^+ and transfer electrons not only to cytochrome b_5 but also to a variety of endogenous and exogenous acceptors. Among the different CYB5R isoforms, a great interest has been paid to CYB5R3 in the fields of metabolism and aging. Alternative splicing of the CYB5R3 gene produces two isoenzymes: a soluble reductase, also known as methaemoglobin reductase, that is restricted to the erythroid lineage, and a membrane-bound isoenzyme which can be ubiquitously found attached to the cytosolic side of the outer mitochondrial membrane (OMM), the endoplasmic reticulum, and the plasma membrane [1].

Membrane-bound CYB5R3 participates in key metabolic processes as the elongation and desaturation of fatty acids [2], biosynthesis of cholesterol and steroid hormones [3], metabolization of xenobiotics [4], reduction of ferric iron in hemeproteins in addition to hemoglobin, as soluble guanylate cyclase (sGC) and myoglobin [1,5,6], and in the recycling of the reduced antioxidant forms of coenzyme Q (CoQ), α-tocopherol and ascorbate [7]. A transplasma membrane redox system that relies on CoQ and CYB5R3 is upregulated by caloric restriction (CR) in mouse liver [8,9] and in cells cultured with sera obtained from animals fed a CR diet [9]. In cellular systems CYB5R3 activity aids in

* Corresponding author. Departamento de Biología Celular, Fisiología e Inmunología, Universidad de Córdoba, Campus de Rabanales, Edificio Severo Ochoa, 3a planta, Campus de Excelencia Internacional Agroalimentario, ceiA3, 14014 Córdoba, Spain.
E-mail addresses: bc2samel@uco.es (L.M. Sánchez-Mendoza), b32pesac@uco.es (C. Pérez-Sánchez), b02rolos@uco.es (S. Rodríguez-López), rosario.lopez.exts@juntadeandalucia.es (C. López-Pedrera), decabora@grc.nia.nih.gov (R. de Cabo), bc1burom@uco.es (M.I. Burón), bc1gorej@uco.es (J.A. González-Reyes), jmvillalba@uco.es (J.M. Villalba).

https://doi.org/10.1016/j.freeradbiomed.2023.07.012
Received 25 April 2023; Received in revised form 14 June 2023; Accepted 11 July 2023
Available online 16 July 2023
0891-5849/© 2023 The Authors. Published by Elsevier Inc. This is an open access article under the CC BY-NC-ND license (http://creativecommons.org/licenses/by-nc-nd/4.0/).

Abbreviations

17aE2	17α-estradiol
Ac-Lys	Acetyl Lysine
CLAP	Chymostatin, Leupeptin, Antipain, and Pepstatin A CLAP
CoQ	Coenzyme Q
CR	Caloric Restriction
CYB5R3	Cytochrome *b*5 reductase 3
DMSO	Dimethyl sulfoxide
DTT	Dithiothreitol
EDTA	Ethylenediaminetetraacetic acid
EGTA	ethylene glycol-bis(β-aminoethyl ether)-N,N,N′,N'-tetraacetic acid
ERα	Estrogen receptor α
HEPES	N-(2-Hydroxyethyl)piperazine-N′-(2-ethanesulfonic acid)
IMFM	intermyofibrillar mitochondria
IMM	inner mitochondrial membrane
Na	number of figures per area
NMR	Nuclear Magnetic Resonance
Nv	Numerical density
OMM	outer mitochondrial membrane
OXPHOS	Oxidative phosphorylation
PMSF	phenylmethylsulphonyl fluoride
RER	respiratory exchange ratio
RIPA	Radioimmunoprecipitation assay
SAEX	Service of Experimentation Animals of the University of Córdoba
sGC	soluble Guanylate Cyclase
SSM	Subsarcolemmal Mitochondria
TG	Transgenic mice overexpressing CYB5R3
TGF	Transgenic Females
TGM	Transgenic Males
TMPD	N,N,N′,N′-tetramethyl-p-phenylenediamine
VCO2	Volume Carbon Dioxide
VO2	Volume Oxygen
Vv	volume density
WTF	Wild-Type Females
WTM	Wild-Type Males
XTOT	total horizontal motor activity
ZTOT	total vertical motor activity

maintaining respiratory metabolism, protects against oxidative stress, prevents cell senescence, increases the cytosolic NAD^+/NADH ratio, and regulates different NAD^+-dependent metabolic pathways [10], supporting that CYB5R3 induction mimics part of CR salutary effects [8,9].

With the aim of exploiting its anti-aging potential, we generated transgenic mice overexpressing CYB5R3 (thereafter referred as TG mice). TG mice not only exhibited several metabolic improvements usually associated to interventions resulting in a healthier phenotype with aging, as better glucose homeostasis, less inflammation, decreased oxidative damage, and protection against induced cancer, but were also found to live longer than their wild-type (WT) counterparts [11]. We also reported for TG mice that CYB5R3 was efficiently overexpressed in skeletal muscle, a postmitotic tissue with a greater contribution to resting energy expenditure [12], and targeted key pathways that modulate the rate of aging, as mitochondrial function, and autophagy [13].

In mammals, longevity is clearly influenced by sex, and lifespan extension in response to anti-aging interventions is also often sex-specific [14]. However, since previous studies involving CYB5R3 overexpression in mice have been carried out with males, it is unknown if sex plays a prominent role in determining the outcome of CYB5R3 overexpression. The aim of the present research was to study the impact of sex on metabolic adaptations elicited by CYB5R3 overexpression in TG mice, and on key markers related with mitochondrial function in skeletal muscle, in comparison with their WT littermates. Our results support that CYB5R3 overexpression induces carbon metabolism adaptations that are distinct in males and in females. Moreover, CYB5R3 overexpression upregulates markers consistent with enhanced mitochondrial biogenesis and function and increases mitochondrial abundance in skeletal muscle, producing most of its potentially beneficial actions in females.

2. Materials and methods

2.1. Generation of CYB5R3-transgenic mice and establishment of mouse cohorts

The rat CYB5R3 gene was cloned in pRC/CMV-rDTD plasmid between cytomegalovirus immediate-early promoter and SV40 polyadenylation sequences [15]. The vector was digested with SwaI and NruI restriction enzymes to cleave the construct, which was then microinjected into fertilized C57BL/6J eggs at the University of Michigan Transgenic Animal Model Core Facility (http://www.med.umich.edu/tamc/). Surviving eggs were transferred to pseudopregnant B6D2F1 female mice. Stable incorporation of the construct into the genome was then validated as previously reported [11]. WT and TG mice were distinguished by PCR genotyping with DNA obtained from tail tissue, using the primers CACCAAAATCAACGGGACTT (forward) and AGACCGGGGAGAGTACCACT (reverse) which reveal the presence of the transgene. An internal control was run in every PCR reaction through the simultaneous amplification of the IL2 gene using the primers CTAGGCCACAGAATTGAAAGATCT (forward) and GTAGGTGGAAATTCTAGCATCATCC (reverse).

TG males were crossed with WT females of the same genetic background (C57BL/6J) purchased from Charles River (Barcelona, Spain). From the resulting offspring, we selected males and females of both genotypes (n = 5–7 per group) and four experimental groups were thus established: WT females (WTF), TG females (TGF), WT males (WTM) and TG males (TGM). The colony was maintained from weaning on 12h light/dark cycle at 22 °C with a free access to water and a standard chow at the Service of Experimentation Animals (SAEX) of the University of Córdoba. Determinations described in this paper were carried out with 3-months old mice.

2.2. Metabolic clamps

Metabolic rate of mice during a fed-fast-refed cycle was assessed by indirect calorimetry in OxyletPro™ metabolic chambers (Panlab, S.L.-Harvard Apparatus, Spain). Animals were housed singly with *ad libitum* access to water and food and maintained at 20–22 °C under a 12:12 h light-dark cycle (light period 07:00–19:00). All mice were acclimatized to monitoring cages for 24 h before the experiments. Constant airflow (0.32–0.36 L/min) was drawn through the chamber and monitored by a mass-sensitive flow meter. The concentrations of O_2 and CO_2 were monitored by sensors placed at the inlet and outlet of the sealed chamber to calculate O_2 consumption and CO_2 release as the difference between the concentrations of these gasses in air entering and leaving the chamber. The sensor was calibrated against a standard gas mix containing defined quantities of O_2, CO_2 and N_2. Data from each chamber were recorded for 2 min at 24-min intervals. Movements (both horizontal and vertical) were also monitored. The system has light beams 1.5 cm apart on the horizontal plane, providing a high-resolution grid covering the XY-planes and the software provides counts of beam breaks by the mouse during 2 min intervals.

2.3. Body composition measurements

Before euthanization (see next paragraph), body composition was measured with a EchoMRI ™ Nuclear Magnetic Resonance (NMR) analyser. After connecting the mouse antenna/sensor insert, the equipment was calibrated with canola oil in accordance with seller specifications. Since animals were not sedated, anesthetized, or restrained during measurements, each mouse was weighed and placed in a transparent support of adjusted size to restrict movements and improve data accuracy. This support was then inserted into the analyser and the scan was carried out for less than 1min to obtain percentages of fat and lean mass, which were used to calculate the lean-to-fat ratio.

2.4. Procurement of tissue samples

When animals reached 3 months, they were anesthetized with isoflurane (at 4% for induction and at 1.5% for maintenance of anaesthesia) with an O_2 flow of 0.8–1 L/min), exsanguinated by cardiac puncture, and finally euthanized by cervical dislocation. Hind limb skeletal muscles were rapidly excised, trimmed from fat and connective tissue, and snap-frozen by immersion in liquid nitrogen in a buffered medium containing 10% DMSO as cryoprotectant. Frozen samples were stored at −80 °C for further analysis. Samples of red gastrocnemius were also obtained and immediately processed for electron microscopy analysis as described below. Procedures with experimentation animals were approved by the bioethics committee of the University of Córdoba and authorized by the *Consejería de Agricultura, Pesca y Desarrollo Rural, Junta de Andalucía, Spain* (authorization code: 06/06/2019/098).

2.5. Preparation of whole tissue extracts

Skeletal muscles were homogenized for 30 s in radioimmunoprecipitation assay (RIPA) buffer containing 50 mM Tris-HCl pH 8, 150 mM NaCl, 0.5% deoxycholate, 0.1% SDS, 1% Triton X-100, 1 mM DTT, 1 mM phenylmethylsulphonyl fluoride (PMSF), 10 μg/mL each of chymostatin, leupeptin, antipain, and pepstatin A (CLAP), and phosphatase inhibitor cocktails 2 and 3 (Sigma-Aldrich) diluted at 1:100, using a mechanical tissue disrupter (Ultra-Turrax T25, IKA, Staufen, Germany) for 30 s. Homogenates were centrifuged at 10,000×*g* for 15min at 4 °C to separate whole protein extracts in the supernatants, which were then transferred to clean tubes and stored frozen at −80 °C until use.

2.6. Isolation of subcellular fractions

Skeletal muscles were dispersed either with an electric tissue disrupter (Ultra-Turrax T25, IKA, Staufen, Germany) for 30s at 4 °C, or with a steel ball mill (MM400, Retsch, Germany) for 5 min at 25 strokes/s using pre-chilled adaptors. The homogenization buffer contained 20 mM Tris–HCl pH 7.6, 40 mM KCl, 0.2 M sucrose, 1 mM PMSF, 10 mM EDTA, 1 mM DTT, 20 μg/μL CLAP, and phosphatase inhibitor cocktails 2 and 3 (Sigma-Aldrich) diluted at 1/100. Homogenates were centrifuged at 420×*g* for 10 min to pellet a cell nuclei and debris-containing fraction that was discarded. Supernatants were collected and centrifuged again at 6700×*g* for 10 min to sediment a heavy membranes (mitochondria-enriched) fraction. These pellets were resuspended in 100 μl of isolation buffer and stored at −80 °C for further analysis. Supernatants derived from this last centrifugation step were transferred to clean ultracentrifuge tubes and spun again at 100,000×*g* for 30 min to separate cytosolic supernatants from pellets containing a fraction of light membranes. Subcellular fractions were tested against the following compartment-specific antibodies: NDUFB8 subunit of complex I (inner mitochondrial membrane, IMM), VDAC (OMM), Na^+/K^+-ATPase (plasma membrane), and procaspase-9 (cytosol). Total amount of protein present in subcellular fractions and in RIPA extracts (see previous section) was estimated using the Bradford dye-binding method as modified by Stoscheck [16].

2.7. Respirometry analysis in isolated skeletal muscle mitochondria

The rate of oxygen consumption by skeletal muscle mitochondria was measured following a recently developed method that allows performing respirometric determinations in mitochondrial fractions isolated from previously frozen tissue [17]. We analysed maximal complex II + III + IV and maximal complex IV-linked respiration in a SeaHorse XFe24 flux analyzer (Agilent, Santa Clara, CA, USA). Briefly, samples of isolated mitochondria containing about 150 μg protein were resuspended in 50 μl of MAS buffer (70 mM sucrose, 220 mM mannitol, 5 mM KH_2PO_4, 5 mM $MgCl_2$, 1 mM EGTA, 2 mM HEPES, pH 7.4), placed in 24-well SeaHorse plates, and centrifuged for 20 min at 4 °C and 3200×*g* in a plate centrifuge (Eppendorf 5810R, Hamburg, Germany) to sediment the mitochondria. Afterwards, 450 μl of MAS buffer were carefully added to each well. Maximal Complex II + III + IV-linked respiration was calculated from the oxygen consumption rate that was stimulated by addition of succinate in the presence of rotenone and then inhibited by antimycin A (final concentrations: 0.65 mM succinate, 0.26 μM rotenone, 0.46 μM antimycin A). Maximal respiration linked solely to Complex IV was calculated from the rate of oxygen consumption that was stimulated by addition of N,N,N′,N′-tetramethyl-p-phenylenediamine (TMPD) plus ascorbic acid and then inhibited by sodium azide (final concentrations: 50 μM TMPD, 0.1 mM ascorbic acid, 4.6 mM azide).

2.8. NAD^+ and NADH determinations

Total tissue levels of NAD^+ and NADH were determined using the NAD^+/NADH-Glo™ bioluminescent assay (Promega, Madison, WI, USA). Skeletal muscle samples were homogenized in an extraction medium composed of PBS:bicarbonate +1% DTAB in a 1:1 ratio, using a MM400 steel ball mill (Retsch, Germany). Specific protocols were then followed to determine separately the levels of NAD^+ or NADH. Thus, homogenate samples containing 10 μg of protein were transferred to 96-well plates and mixed with either an acidic or a basic medium in a final volume of 50 μl. In the last step, 8 μl of each mixture were transferred to 384-well plates and combined with an equivalent volume of "Ultra-Glo™ rLuciferase" reagent. Once incubated at room temperature for 30–60 min, the luminometric signal of the samples was read in a Tecan Infinite 200 PRO plate Luminometer (Switzerland).

2.9. Electrophoresis and western blot immunodetection

Electrophoresis and electro-transference to nitrocellulose sheets were carried out as described previously [18]. Membranes were then probed against the primary antibodies listed in Table 1. The corresponding species-specific secondary antibodies coupled to horseradish peroxidase were used to reveal binding sites by enhanced chemiluminescence (ClarityTM Western ECL Blotting Substrates Kit, Bio-Rad). Chemiluminescence signals were recorded using a ChemiDoc Imaging System (Bio-Rad), and the densitometric quantification of immunostained bands was carried out with Image LabTM Software (Bio-Rad). Data were normalized to the overall image density of the corresponding lane stained with Ponceau S. All samples depicted in each figure were run on the same gel. In case a misplacement of specific samples during electrophoresis was detected, the corresponding band was placed within its group without any further alteration of the image.

2.10. Ultrastructural analysis of skeletal muscle mitochondria

Samples of red gastrocnemius were fixed in a mixture of 2.5% glutaraldehyde–2% paraformaldehyde in 0.1 M sodium cacodylate buffer pH 7.2 for 12–24 h and then washed in buffer and post fixed in 1% osmium tetroxide for 1 h at 4 °C in the same buffer. Tissue pieces were

Table 1
Primary antibodies used in this study. The table shows the concentrations and the commercial references of each antibody. (SC: Santa Cruz Antibodies).

Primary Antibodies	Dilution	Reference	Primary Antibodies	Dilution	Reference
CYB5R3	1:1000	Proteintech 10894-1-AP	**DRP-1**	1:500	SC-32898
PINK1	1:1000	SC-33796	**FIS-1**	1:500	SC-98900
PARKIN	1:100	Cell Signaling 2132	**Caspase-9**	1:1000	SC-8355
NRF-1	1:2000	SC-33771	**VDAC**	1:1000	SC-98708
OxPhos rodent WB antibody cocktail[a]	1:4000	Life technologies 458,099	**TFAM**	1:1000	SC-2358
MFN-1	1:1000	SC-50330	**SIRT-1**	1:1000	SC-15404
MFN-2	1:500	SC-50331	**SIRT-3**	1:1000	SC-99143
Ac-Lys	1:1000	SC-32852	**Na^+/K + -ATPase**	1:1000	SC-16041
Cytochrome *c*	1:1000	BD Pharmingen™ 556,433	**HIF-1 α**	1:1000	SC-10790
HO-1	1:1000	Cell Signaling 70081S			

[a] OxPhos rodent WB antibody cocktail:Complex I subunit NDUFB8 (NADH dehydrogenase (ubiquinone) 1 beta subcomplex subunit 8)Complex II subunit SDHB (Succinate dehydrogenase (ubiquinone) iron-sulfur subunit)Complex III subunit UQCRC2 (Cytochrome *b*-*c*1 complex subunit)Complex IV subunit MTCO1 (mitochondrially encoded cytochrome *c* oxidase I)Complex V subunit ATP5A (Complex V alpha subunit).

dehydrated in an ascending series of ethanols, transferred to propylene oxide, and then infiltrated in EMbed 812 resin (Electron Microscopy Sciences, PA, USA) using the sequence: propylene oxide:resin 2:1, 1:1, and 1:2 throughout 24 h (8 h each), and pure resin for 24 h. After infiltration, tissue pieces were transferred to silicon molds containing fresh resin, and oriented to obtain cross sections. Finally, blocks were allowed to polymerize for 48 h at 65 °C.

Blocks were trimmed from excess resin and sectioned in an Ultracut Reicher ultramicrotome. Thin sections (40–70 nm thick) were mounted on nickel grids and stained in uranyl acetate and lead citrate. Stained sections were examined and photographed in a Jeol JEM 1400 electron microscope at the Servicio Centralizado de Apoyo a la Investigación (SCAI; University of Córdoba; Spain). Micrographs were taken randomly at 20,000X from both peripheral and internal zones of the cells and used for planimetric (sectional area and circularity) and stereological analyses of mitochondria. Stereological analyses were performed to calculate volume density (Vv), defined as the volume occupied by mitochondria per volume unit of the cell (expressed in $\mu m^3/\mu m^3$), and numerical profile density (Na), which measures the number of mitochondria per μm^2 of cell surface. To this purpose, we followed the point counting method of Weibel [19] by superposing the pictures with a simple square lattice with 0.4 μm separation between points. All measurements were performed using ImageJ software (NIH).

2.11. Statistical analysis

Data were expressed as mean ± SEM. The Kolmogorov-Smirnov test was employed to assess for values normality. Means were compared by two-tailed Student's *t*-test, whereas global effects of age or genotype were assessed by two-way ANOVA. In case data did not pass the normality test, the nonparametric two-tailed Mann–Whitney test was followed. Differences in mitochondrial size among experimental groups were evaluated by frequency distribution analysis of at least 1000 mitochondria profiles from each group. Size distributions were compared by means of the nonparametric Kolmogorov-Smirnov test. Significant differences were expressed as follows: * ($p < 0.05$), **($p < 0.01$), *** ($p < 0.001$) and **** ($p < 0.0001$). All statistical analyses and graphics were performed using GraphPad Prism 8 (GraphPad Software Inc., San Diego, CA).

3. Results

3.1. Metabolic and behavioural responses in WT and TG males and females

We first studied body weight and composition in 3mo-old males and females of WT or TG genotype. As expected [20], males showed higher body weight than females. This difference was independent on the genotype, although we found a trend towards a higher body weight in TGF when compared with WTF (Supplemental Fig. 1A). Differences between males and females were also highlighted for body composition: overall, higher lean and lower fat mass were seen in males (and, accordingly, lean-to-fat ratio values were also higher in males than in females) regardless genotype. However, in contrast with our previous findings obtained with mice at a more advanced age (9–10 months), we did not evidence statistically significant differences between genotypes for any of these parameters (Supplemental Figs. 1B–D).

We also submitted mice of both sexes and genotypes to indirect calorimetry determinations in separate metabolic chambers to provide estimates of energy expenditure during a feeding-fasting-refeeding cycle (see Fig. 1 and Supplementary Fig. 2A). No statistically significant differences among genotypes were found in males throughout the whole feeding-fasting-refeeding cycle, but we found a trend towards decreased respiratory exchange ratio (RER) in TGM compared with WTM during some periods of the feeding-fast-refeeding cycle (Fig. 1A, right) which was due to a slight increase in VO_2 (Fig. 1B, right) without changes in VCO_2 (Fig. 1C, right). TGF exhibited higher RER than WTF during the light period of the first feeding cycle (Fig. 1A, left) due to a slight increase in VCO_2 (Fig. 1C, left) that was not accompanied by a change in VO_2 (Fig. 1B, left).

When comparisons were made for sex, RER values were in general higher in females than in males regardless genotype (Fig. 1A), with increased consumption of O_2, particularly during the light period of the refeeding cycle (Fig. 1B), and release of CO_2 (Fig. 1C). Nevertheless, differences in spontaneous ambulatory activity between males and females over the course of the fed-fasted–refed cycle (irrespective of genotype) did not reach statistical significance (Supplementary Fig. 2B). Regarding genotypes, we only encountered higher Ztot counts in WT males compared with TG males (Supplementary Fig. 2B, right). No differences among sexes or genotypes were found for food consumption (Supplementary Fig. 2D), while TGM exhibited a slight decrease in water consumption compared with TGF (Supplementary Fig. 2E).

3.2. Targeting of ectopic CYB5R3 to subcellular compartments in skeletal muscle is not altered by sex

We obtained subcellular fractions that were enriched in mitochondria, microsomes plus plasma membranes, and cytosol, respectively, as demonstrated from their staining patterns with specific antibodies raised against compartment-specific protein markers (see Supplemental Information and Supplemental Fig. 3). We observed a conspicuous pattern of CYB5R3 overexpression in skeletal muscle homogenates from TG mice, and the accrual of CYB5R3 polypeptide was independent on sex. Despite this lack of differences between sexes in TG mice, we evidenced sexual dimorphism for the abundance of endogenous CYB5R3 in skeletal muscle homogenates since, although being present at much lower levels that in TG mice, the amounts of endogenous CYB5R3 in skeletal muscle homogenates were significantly higher in WTF than in

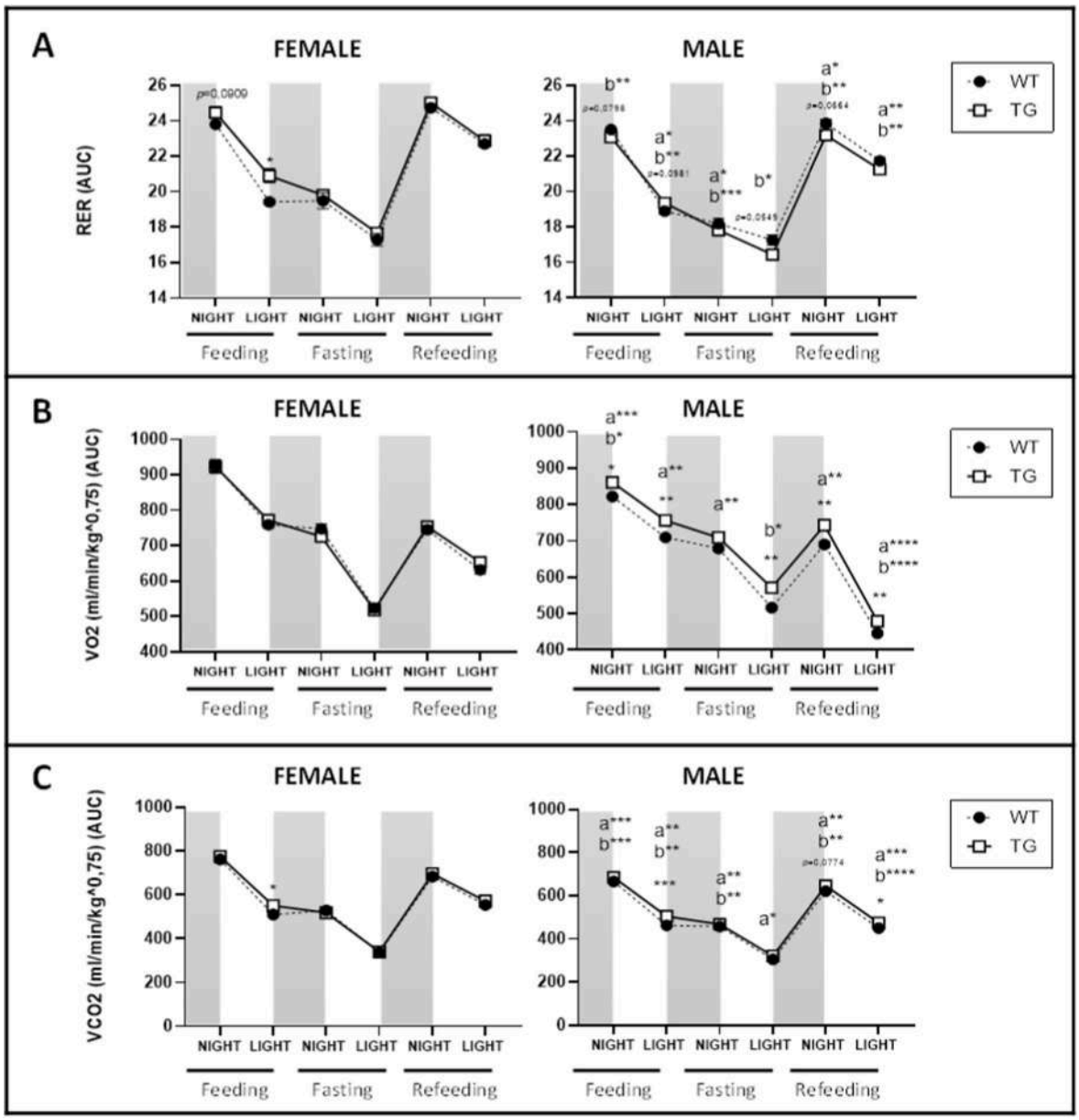

Fig. 1. Indirect respiration calorimetry. Plots depict the respiratory exchange ratio (RER) (A), volume of O_2 consumed (B) and volume of CO_2 produced (C) in females and males of WT or CYB5R3 genotypes during a fed-fast-refed cycle. Night/light cycles are represented in panels by alternate gray/white bars. Asterisks above each cycle denote the level of significance of the differences between genotypes (WT *vs.* TG) for a given sex, whereas a trend is denoted by *p* value. Asterisks that are accompanied by "a" (for WT) or "b" (for TG) denote significant differences between females and males for a given genotype, whereas a trend is denoted by *p* value accompanied by these same letters. Data are shown as AUC ± SEM of 4–5 animals per group. Means were compared by Student's *t*-test.

WTM (Fig. 2A and D).

In subcellular fractions, we observed a significant accumulation of CYB5R3 polypeptide both in mitochondria-enriched low-speed precipitates (Fig. 2B and D) and in microsomes plus plasma membrane-enriched, high-speed precipitates (Fig. 2C and D) from TG mice, with the highest levels being reached in the former. CYB5R3 was not detected in cytosol-enriched high-speed supernatants (Fig. 2D). The abundance of CYB5R3 protein in membranous fractions paralleled that measured in homogenates and thus, differences between sexes were neither evidenced here (Fig. 2B and C). Fig. 2D depicts western blots used for quantification of CYB5R3 protein levels with their corresponding Ponceau S-stained lanes used for normalization of protein loading.

3.3. NAD^+ and NADH levels in skeletal muscle exhibit sexual dimorphism and can be modulated by CYB5R3 overexpression

Both NADH and NAD^+ contents were higher in females that in males regardless genotype (Fig. 3A and B). Whereas CYB5R3 overexpression increased significantly NADH, both in females and males (Fig. 3B), no statistically significant variations among experimental groups were found in the NAD^+/NADH ratio (Fig. 3C).

3.4. CYB5R3 overexpression regulates the abundance of mitochondrial complexes markers and cytochrome c in a sex-specific way

We found a general increase of the mitochondrial oxidative phosphorylation complexes in the males independently on genotype, except for complex II which was found increased in females (Fig. 4A–E). The

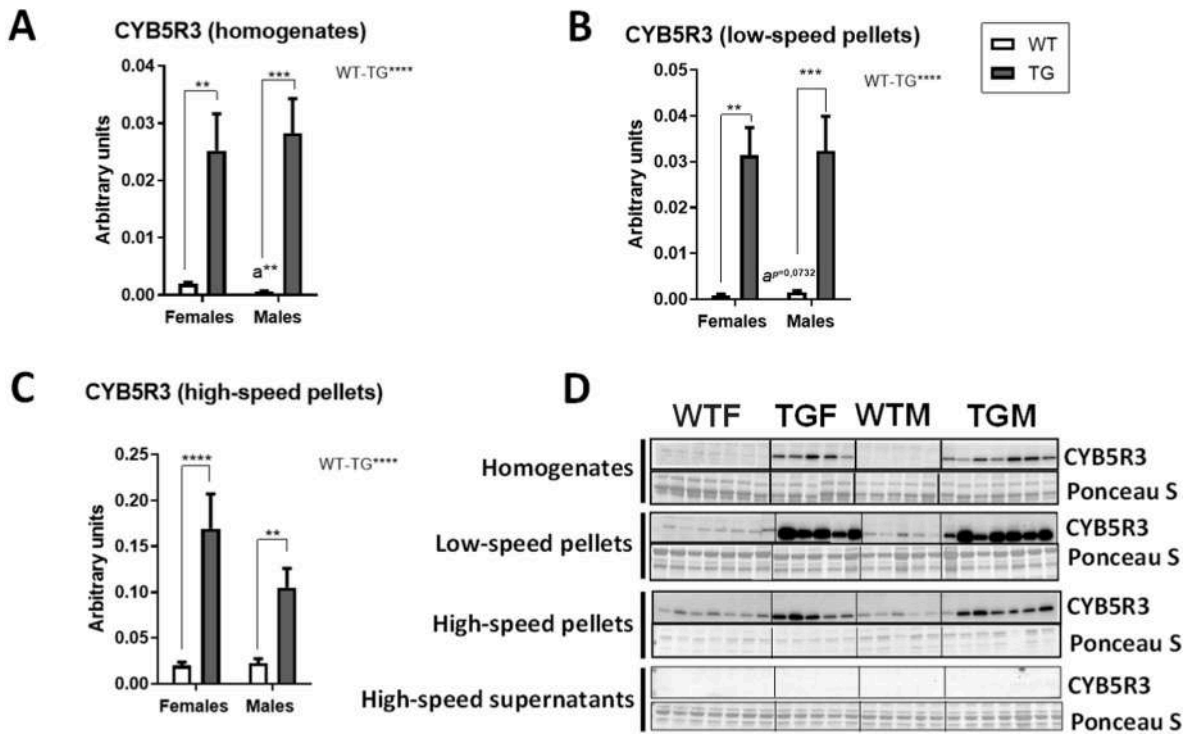

Fig. 2. Expression levels of CYB5R3 polypeptide in hind-limb skeletal muscles from male and female mice of WT and TG genotypes. The figure depicts CYB5R3 levels in homogenates (A), low-speed (mitochondria-enriched) pellets (B), and high-speed (microsomes plus plasma membranes-enriched) pellets (C). Panel D shows western blots used for quantification of protein levels with their corresponding Ponceau S-stained lanes used for normalization of protein loading. Asterisks in the bars denote the level of significance of the differences between genotypes (WT *vs*. TG) for a given sex. Global effects of genotype (regardless of sex) are represented as "WT-TG" with asterisks. Data are shown as means ± SEM of 5–7 animals per group. Global effects of age or genotype were evaluated by two-way ANOVA. Means in panels A and B were compared by Mann–Whitney nonparametric test, whereas those in panel C were compared by Student's *t*-test.

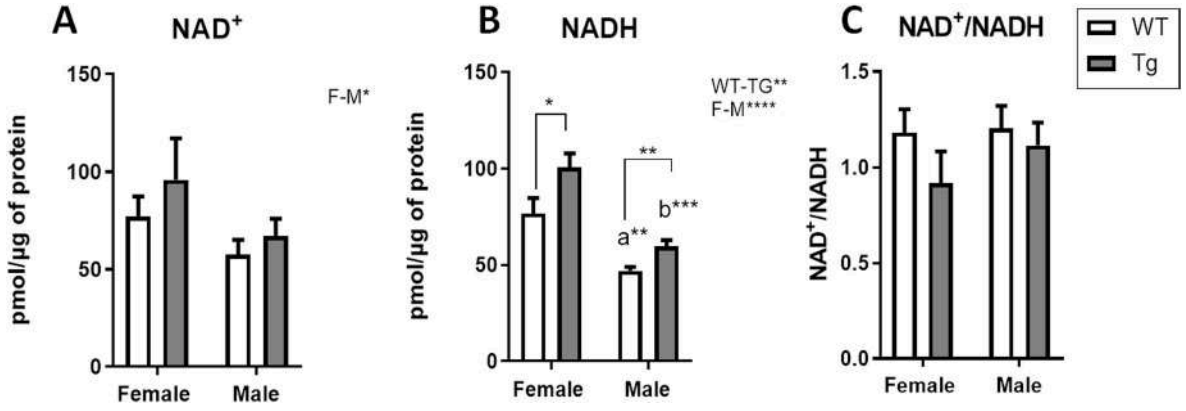

Fig. 3. Levels of NAD^+ (A) and NADH (B), and NAD^+/NADH ratio (C) in hind-limb skeletal muscles from female and male mice of WT and TG genotypes. Asterisks in the bars denote the level of significance of the differences between genotypes (WT *vs*. TG) for a given sex. Asterisks that are accompanied by "a" (for WT) or "b" (for TG) denote significant differences between females and males for a given genotype, whereas a trend is denoted by *p* value accompanied by these same letters. Global effects of sex (regardless of genotype) are represented as "F-M" with asterisks, while overall effects of genotype (regardless of sex) are represented as "WT-TG" with asterisks. The interaction "sex x genotype" is also indicated when appropriate. Data are shown as means ± SEM of 7 animals per group. Global effects of age or genotype were evaluated by two-way ANOVA. Means were compared by Student's *t*-test.

increase of mitochondrial complexes abundance in the males was particularly marked for complex IV (Fig. 4D). On the other hand, CYB5R3 overexpression increased the abundance of complexes I, II and III markers, and this effect was more conspicuous in males than in females (Fig. 4A, B and 4C). However, CYB5R3 overexpression upregulated cytochrome *c* specifically in females (Fig. 4F). Fig. 4G depicts western blots used for quantification of mitochondrial complexes markers and cytochrome *c* with their corresponding Ponceau S-stained lanes used for normalization of protein loading.

3.5. CYB5R3 overexpression enhances maximal respiration by isolated mitochondria in females

We next wanted to ascertain if sex and/or CYB5R3 overexpression produced changes in the rates of mitochondrial respiration. Interestingly, while we did not evidence statistically significant differences between males and females, CYB5R3 overexpression led to a significant increase of maximal Complex IV-linked oxygen consumption in females, and a trend towards higher maximal Complexes II + III + IV-linked

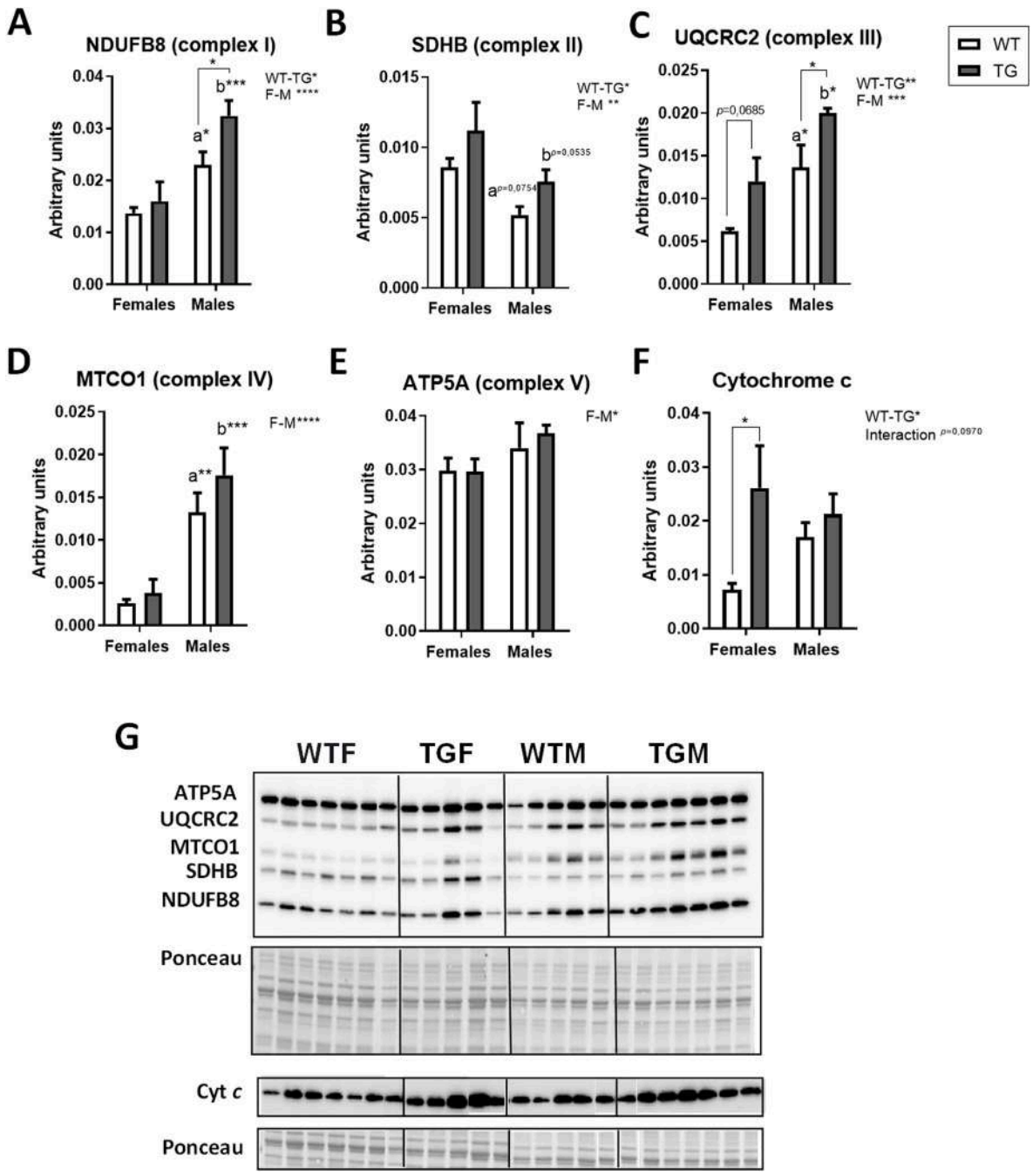

Fig. 4. Abundance of selected markers for mitochondrial electron transport chain complexes and levels of cytochrome *c* in hind-limb skeletal muscles from female and male mice of WT and TG genotypes. Panels A to E represent the levels of mitochondrial complexes I to V, respectively. Panel F shows cytochrome *c* levels. Panel D shows western blots used for quantification of protein levels with their corresponding Ponceau S-stained lanes used for normalization of protein loading. Asterisks in the bars denote the level of significance of the differences between genotypes (WT *vs.* TG) for a given sex. Asterisks that are accompanied by "a" (for WT) or "b" (for TG) denote significant differences between females and males for a given genotype, whereas a trend is denoted by *p* value accompanied by these same letters. Global effects of sex (regardless of genotype) are represented as "F-M" with asterisks, while overall effects of genotype (regardless of sex) are represented as "WT-TG" with asterisks. The interaction "sex x genotype" is also indicated when appropriate. Data are shown as means ± SEM of 5–7 animals per group. Global effects of age or genotype were evaluated by two-way ANOVA. Means in panels A, B and F were compared by Student's *t*-test, whereas those in panels C, D and E were compared by Mann–Whitney nonparametric test.

respiration was observed as well (Fig. 5A and B). However, no effects on maximal oxygen consumption were evidenced in mitochondria isolated from males (Fig. 5C and D). Fig. 5E depicts the results of a representative respirometry assay with isolated mitochondria, as measured with the SeaHorse XFe24 flux analyzer.

3.6. CYB5R3 overexpression upregulates markers of mitochondrial dynamics, biogenesis, mitophagy and oxidative capacity in skeletal muscle from females without affecting HIF1

We next investigated the impact that sex and/or CYB5R3 overexpression impose on mitochondrial dynamics by studying the levels of key marker proteins related with mitochondrial fusion and fission

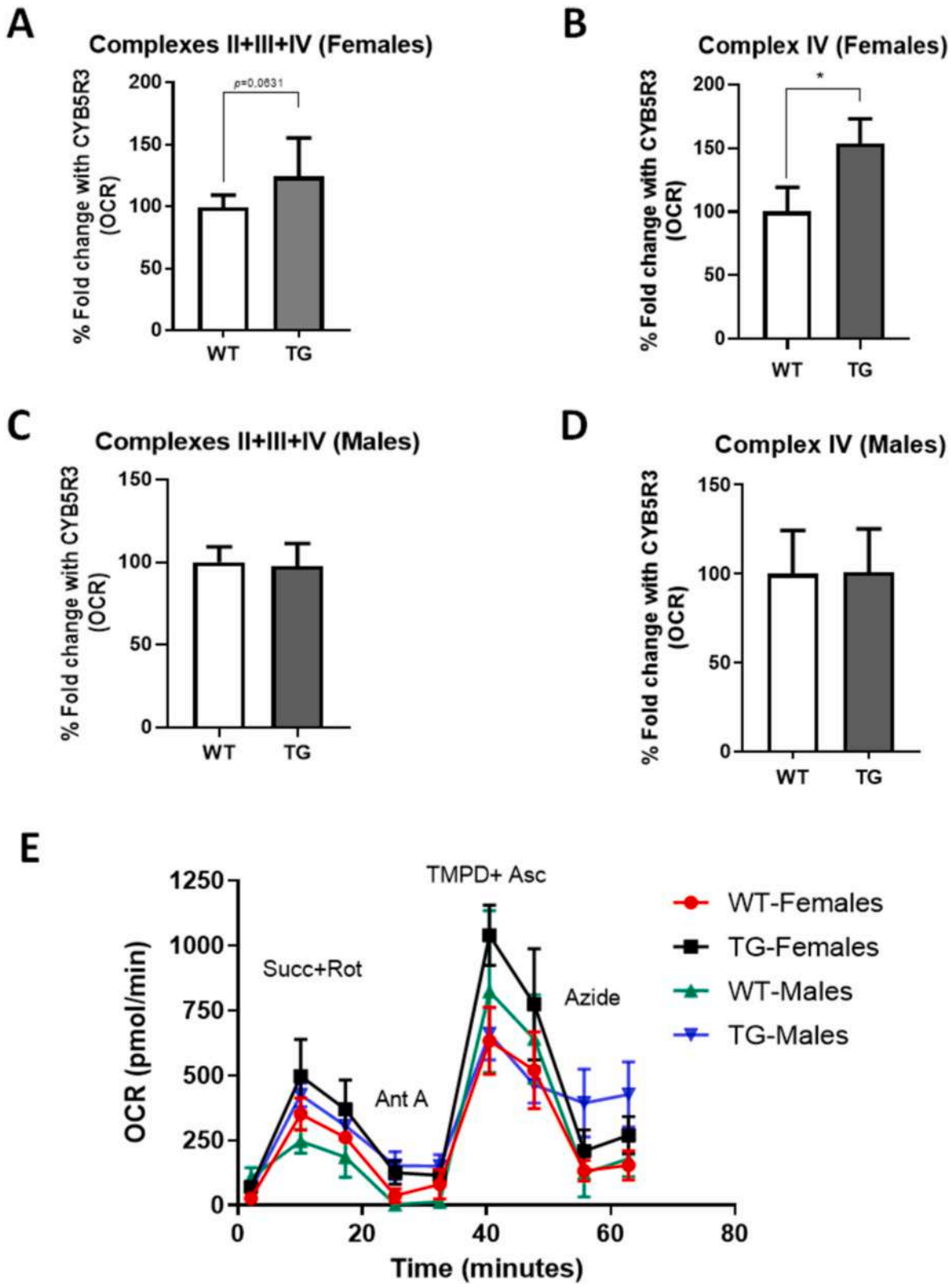

Fig. 5. Respirometry measurements with enriched mitochondrial fractions. Panel A: Complexes II + III + IV-dependent respiration by mitochondria isolated from skeletal muscles of females. Panel B: Complex IV-dependent respiration by mitochondria isolated from skeletal muscles of females. Panel C: Complexes II + III + IV-dependent respiration by mitochondria isolated from skeletal muscles of males. Panel D: Complex IV-dependent respiration by mitochondria isolated from skeletal muscles of males. Panel E: a representative respirometry assay as measured in the SeaHorse flux analyzer. Asterisks in the bars denote the level of significance of the differences between genotypes (WT *vs*. TG) for a given sex, whereas a trend is denoted by *p* value. Data in panels A, B and C are shown as means ± SEM of 10 animals per group. OCR: oxygen consumption rate, Succ: succinate, Rot: rotenone. Means were compared by Student's *t*-test.

phenomena. The mitofusins MFN-1 and MFN-2 were measured as fusion markers whereas FIS-1 and DRP-1 were measured as fission markers. No statistically significant differences between groups were detected for the two mitofusins, with the sole exception of a trend towards decreased MFN-1 in TGM compared with TGF (Fig. 6A and B). However, regarding the fission markers we evidenced a significant increase of DRP-1 in TGF, but not in TGM, with respect to each corresponding WT control. A trend towards increased DRP-1 was also observed in WTM in comparison with WTF (Fig. 6C). Conversely, levels of FIS-1 were significantly higher in WTF with respect to WTM (Fig. 6D). No sexual dimorphism was evidenced for both fission markers in TG mice (Fig. 6C and D). Fig. 6E depicts western blots used for quantification of protein levels with their corresponding Ponceau S-stained lanes used for normalization of protein loading.

We next measured the levels of TFAM and NRF1, two key transcription factors regulating mitochondrial biogenesis. The abundance of both TFAM and NRF1 polypeptides in skeletal muscle homogenates was found regulated both by sex and by CYB5R3 overexpression. As illustrated in Fig. 7A, TFAM was upregulated in WTM in comparison with WTF. Of note, how CYB5R3 overexpression affected TFAM levels was highly dependent on sex since it was upregulated in TGF but downregulated in TGM. As a result, the sex-dependent differences in TFAM abundance seen in WT mice were abated in mice overexpressing CYB5R3. Regarding NRF1, we also evidenced its upregulation by

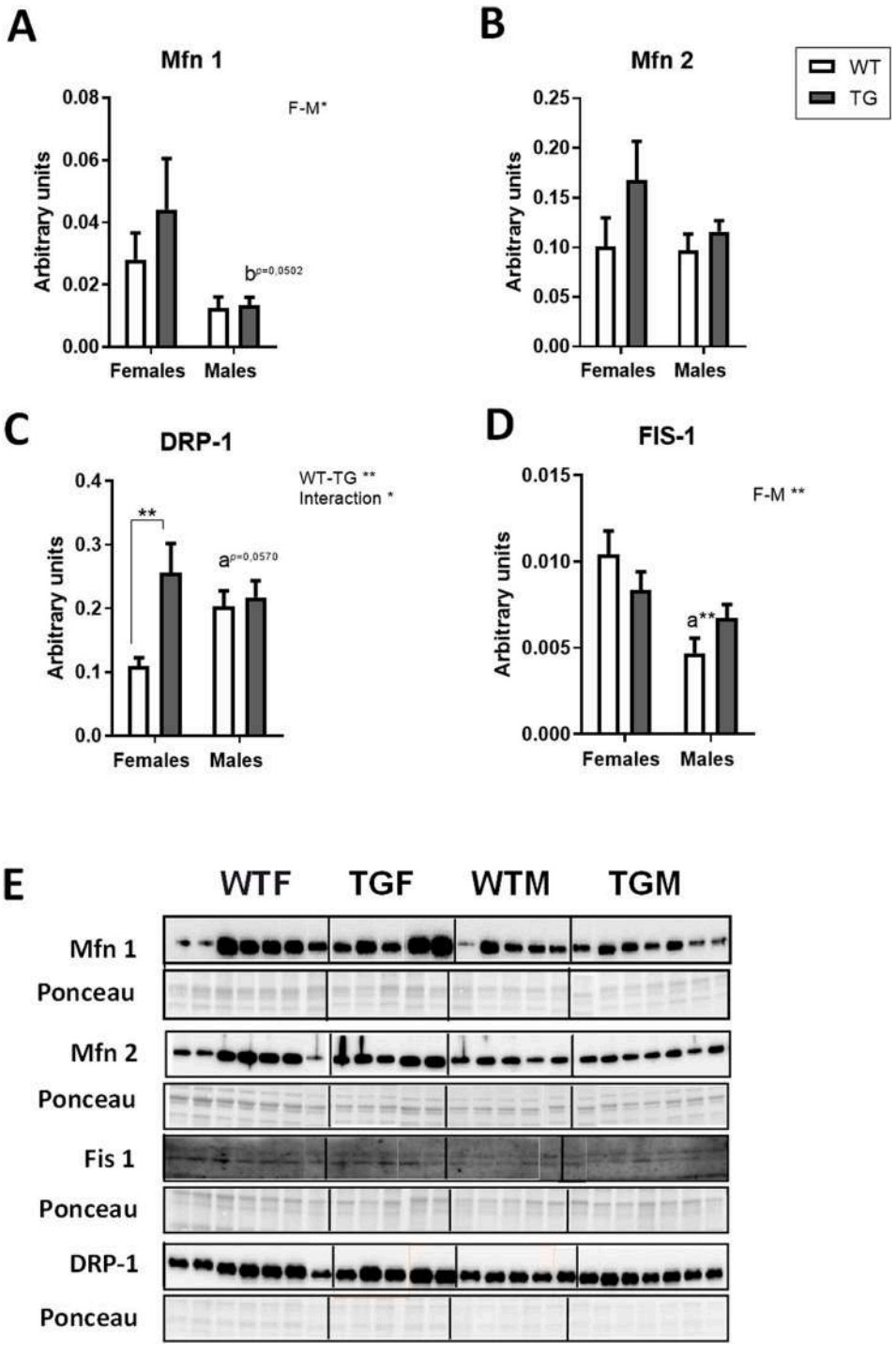

Fig. 6. Expression levels of proteins related to mitochondrial fusion and fission: MFN-1 (A), MFN-2 (B), DRP-1 (C) and FIS-1 (D) in hind-limb skeletal muscles from female and male mice of WT and TG genotypes. Panel E shows western blots used for quantification of protein levels with their corresponding Ponceau S-stained lanes used for normalization of protein loading. Asterisks in the bars denote the level of significance of the differences between genotypes (WT *vs.* TG) for a given sex. Asterisks that are accompanied by "a" denote significant differences between females and males of WT genotype, whereas a trend is denoted by *p* value accompanied by the same letter. Global effects of sex (regardless of genotype) are represented as "F-M" with asterisks, while overall effects of genotype (regardless of sex) are represented as "WT-TG" with asterisks. The interaction "sex x genotype" is also indicated when appropriate. Data are shown as mean ± SEM of 5–7 animals per group. Global effects of age or genotype were evaluated by two-way ANOVA. Means were compared by Student's *t*-test.

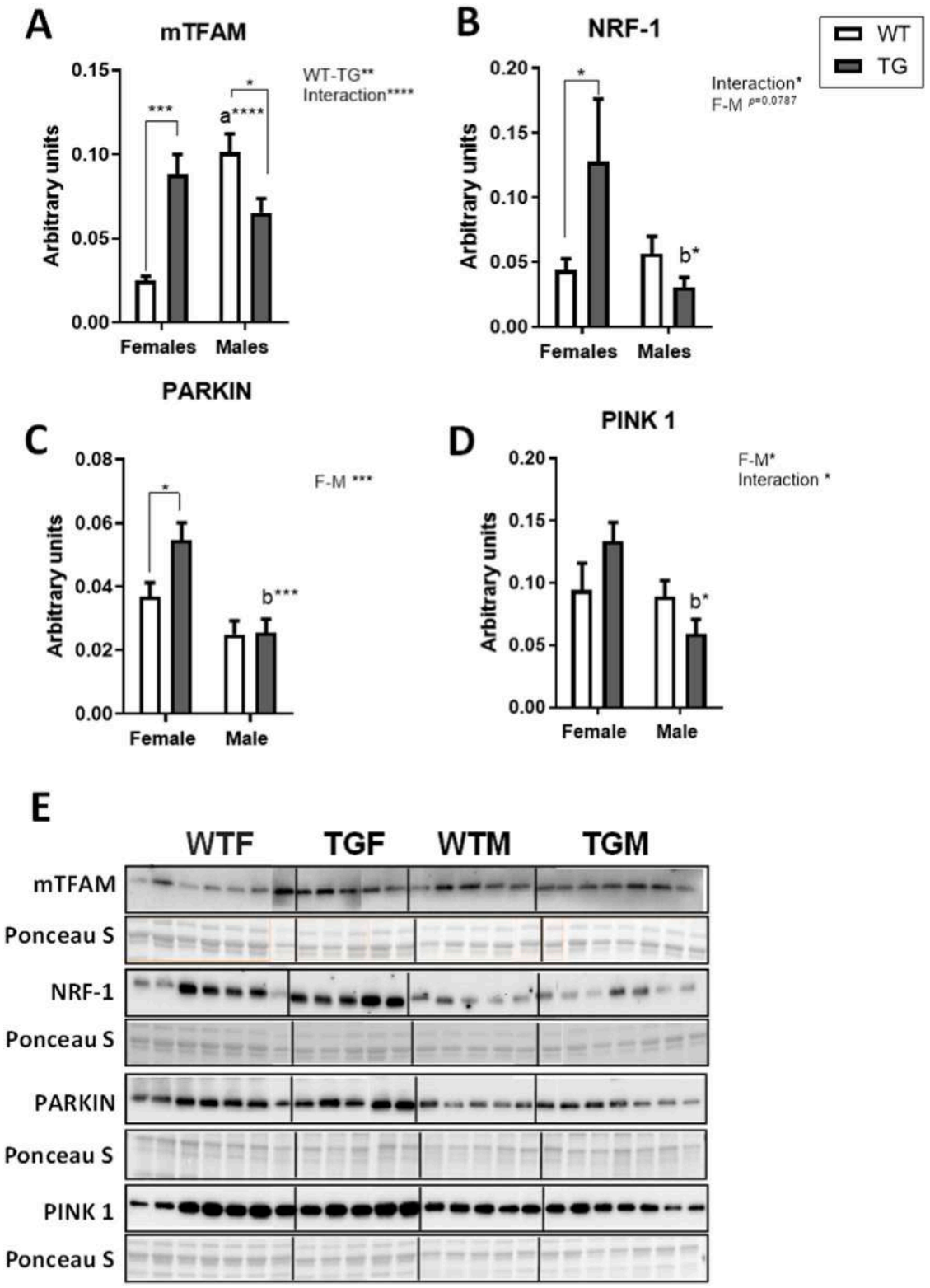

Fig. 7. Expression levels of proteins related to mitochondrial biogenesis and mitophagy: TFAM (A), NRF-1 (B), PARKIN (C) and PINK-1 (D) in hind-limb skeletal muscles from female and male mice of WT and TG genotypes. Panel E shows western blots used for quantification of protein levels with their corresponding Ponceau S-stained lanes used for normalization of protein loading. Asterisks in the bars denote the level of significance of the differences between genotypes (WT *vs*. TG) for a given sex. Asterisks that are accompanied by "b" denote significant differences between females and males of TG genotype. Global effects of sex (regardless of genotype) are represented as "F-M" with asterisks, and overall effects of genotype (regardless of sex) are represented as "WT-TG" with asterisks, whereas a trend is denoted by *p* value. The interaction "sex x genotype" is also indicated when appropriate. Data are shown as mean ± SEM of 5–7 animals per group. Global effects of age or genotype were evaluated by two-way ANOVA. Means were compared by Student's *t*-test, whereas those in panel A were compared by Mann–Whitney nonparametric test.

CYB5R3 overexpression in females, whereas no effect was observed in males. In this case, sexual polymorphism was observed in TG but not in WT mice, with TGF showing significantly higher levels of NRF1 than TGM (Fig. 7B).

Regarding two of the most relevant proteins involved in the autophagic clearance of mitochondria (mitophagy), we found no differences between WTM and WTF in the levels of PARKIN and PINK1, but a significant increase of both proteins was observed in TGF when compared with TGM (Fig. 7C and D). Of note, PARKIN was upregulated by CYB5R3 overexpression in females but not in males (Fig. 7C), as we had also evidenced for TFAM and NRF1 (see above). Fig. 7E depicts western blots used for quantification of protein levels with their corresponding Ponceau S-stained lanes used for normalization of protein loading.

SIRT3 has been linked to both oxidative capacity and mitochondrial density in cell lines and in mammalian tissues [21]. Thus, we also wanted to investigate the effects of sex and/or CYB5R3 overexpression on SIRT3. Besides its cleaved (mitochondrial) isoform, we also included in our study the full-length SIRT3, located in the nucleus in cell lines [22], and SIRT1, another key regulator of mitochondrial biogenesis in skeletal muscle [23]. Interestingly, the pattern of mitochondrial SIRT3 changes with sex and/or CYB5R3 overexpression (Fig. 8A) closely resembled that of TFAM, suggesting that metabolic effects of CYB5R3 overexpression in skeletal muscle not only affected mitochondrial biogenesis but also its oxidative capacity. Unlike the SIRT3 cleaved isoform, the full-length protein exhibited no change due to CYB5R3 overexpression, and we only observed a trend towards a decrease in TGM in comparison with TGF (Supplemental Fig. 4). SIRT1 was found upregulated in males independently of CYB5R3 overexpression which did not produce any effect on its abundance (Fig. 8B). Fig. 8C depicts western blots used for quantification of protein levels with their corresponding Ponceau S-stained lanes used for normalization of protein loading.

Since we had encountered some differences in the levels of the deacetylases SIRT1 and SIRT3 among experimental groups, we wanted to test if these differences were translated into changes of pan-acetylation of proteins, which were measured both in whole skeletal muscle extracts and in mitochondria-enriched fractions. As shown in Fig. 8C, CYB5R3 overexpression produced an increase in the pan-acetylation of proteins in the homogenates independently of sex, although acetylation levels were higher in males than in females. When the measurements were carried out with isolated mitochondria, acetylation levels were hound higher in WTM compared with WTF. CYB5R3 overexpression significantly increased protein acetylation in females but not in males and, as a result, sexual differences were abated in TG mice (Fig. 8D). Fig. 8E depicts western blots used for quantification of protein levels with their corresponding Ponceau S-stained lanes used for normalization of protein loading.

We did not evidence any significant change in HIF1 abundance either with sex or with CYB5R3 overexpression (Fig. 9A). However, HO-1 was found increased in males compared with females regardless genotype and, interestingly, was dramatically upregulated by CYB5R3 overexpression in males but not in females (Fig. 9B).

3.7. The regulation of mitochondrial size and abundance in skeletal muscle by CYB5R3 overexpression is sex-specific

In cross-sections from red fibres, we found that the mean size of intermyofibrillar mitochondria (IMFM) was higher in WTM when compared with WTF. Interestingly, the size of these type of mitochondria was increased by CYB5R3 overexpression in females but decreased in males (Fig. 10A). No change in the size of subsarcolemmal mitochondria (SSM) was observed for any of the experimental groups (Fig. 10B).

The analysis of size distributions of mitochondrial profiles showed us that the higher size of IMFM we had observed in both TGF and WTM in comparison with the other two groups (as shown in Fig. 10A) was due to the enrichment in a mitochondrial population measuring about 0.25 μm^2, concomitant with a decrease in a population measuring about 0.04 μm^2 in cross-sections (Supplemental Fig. 5A). Conversely, the abundance of these two populations was reversed in WTF and TGM (Supplemental Fig. 5A), which resulted in the decrease of mean size observed for these two groups. Regarding SSM, whereas the comparison of mean size values had not revealed statistically significant differences among

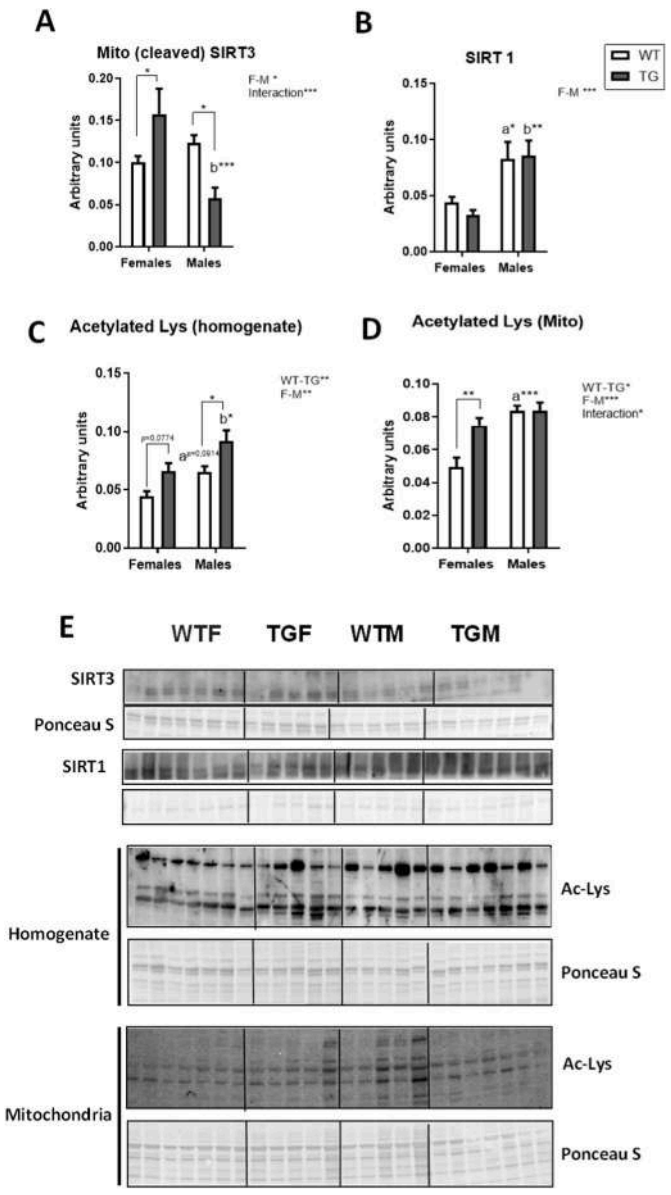

Fig. 8. Abundance of cleaved (mitochondrial) SIRT3 (A) and SIRT1 (B) and protein pan-acetylation in homogenates (C) and enriched mitochondrial fractions (D) in hind-limb skeletal muscles from female and male mice of WT and TG genotypes. Panel E shows western blots used for quantification of protein levels with their corresponding Ponceau S-stained lanes used for normalization of protein loading. Asterisks in the bars denote the level of significance of the differences between genotypes (WT *vs*. TG) for a given sex, whereas a trend is denoted by *p* value. Asterisks that are accompanied by "a" (for WT) or "b" (for TG) denote significant differences between females and males for a given genotype. Global effects of sex (regardless of genotype) are represented as "F-M" with asterisks, while overall effects of genotype (regardless of sex) are represented as "WT-TG" with asterisks. The interaction "sex x genotype" is also indicated when appropriate. Data are shown as means ± SEM of 5–7 animals per group. Global effects of age or genotype were evaluated by two-way ANOVA. Means were compared by Student's *t*-test.

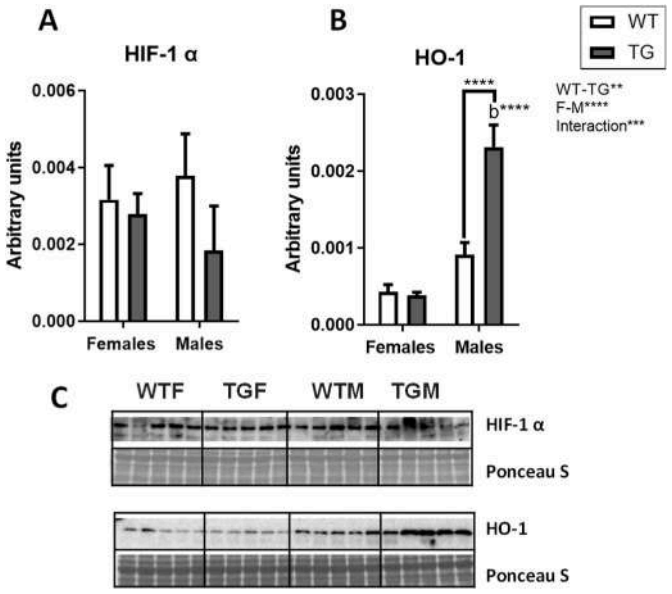

Fig. 9. Abundance of HIF-1 (A) and HO-1 (B) in hind-limb skeletal muscles from female and male mice of WT and TG genotypes. Panel C shows western blots used for quantification of protein levels with their corresponding Ponceau S-stained lanes used for normalization of protein loading. Asterisks in the bars denote the level of significance of the differences between genotypes (WT *vs.* TG) for a given sex. Asterisks that are accompanied by "b" denote significant differences between TG females and TG males. Global effects of sex (regardless of genotype) are represented as "F-M" with asterisks, while overall effects of genotype (regardless of sex) are represented as "WT-TG" with asterisks. The interaction "sex x genotype" is also indicated with its level of significance. Data are shown as means ± SEM of 5–7 animals per group. Global effects of age or genotype were evaluated by two-way ANOVA. Means were compared by Student's *t*-test.

groups, size distribution of mitochondrial profiles in WTM deviated significantly from the distributions of the remaining groups, due to an underrepresentation of profiles with sizes ranging from about 0.1 μm^2 to about 0.16 μm^2 in WTM. Consequently, statistically significant differences were highlighted for WTM in comparison with both WTF and TGM, while no differences in size distributions were observed for WTF *vs.* TGF, and for TGF *vs.* TGM (Supplemental Fig. 5B).

Values of circularity, a parameter related with shape, did not differ between males and females of WT genotype but CYB5R3 overexpression decreased circularity of IMM in females. As a result, IMFM circularity was lower in TGF than in TGM (Fig. 10C). No statistically significant differences in circularity were observed for SSM among any of the experimental groups (Fig. 10D). Regarding the stereological parameters applied to mitochondria, Vv values were unchanged among experimental groups (Fig. 10E) but Na, a marker of numerical abundance, was significantly increased by CYB5R3 overexpression in the females (Fig. 10F). Representative micrographs of cross-sections from all experimental groups are shown in Supplemental Fig. 5.

4. Discussion

Since our first demonstration that CYB5R3 overexpression improves metabolism and prolongs lifespan in mice [11], we have further extended our work to elucidate the tissue-specific response to CYB5R3 overexpression, the interaction between CYB5R3 overexpression and other pro-longevity interventions as CR, and the effect of aging on TG mice. In this sense, the accrual of CYB5R3 polypeptide in TG mice is tissue-specific, with skeletal muscle exhibiting greater enrichment of CYB5R3 polypeptide over liver and kidney [11,13,24]. While CYB5R3 overexpression mimics by itself some of the salutary outcomes of CR, their mechanisms of action are not coincidental [11], and CYB5R3 overexpression can be even significantly modify the metabolic adaptations to CR in TG mice, preventing MFN-2 and TFAM upregulation by CR in liver, and mitochondrial mass increase in skeletal muscle [24]. Nevertheless, CYB5R3 overexpression by itself protects against some aging-associated biochemical and structural alterations in mitochondria and modulates autophagic signalling in skeletal muscle [13].

Despite these progresses, the possible involvement of sex as a factor that also determines the outcome of CYB5R3 overexpression remains unexplored. In mammals, both longevity and lifespan extension in response to anti-aging interventions can be strongly influenced by sex [14]. For instance, while rapamycin increases lifespan in both male and female mice [25–27], the benefits of 17α-estradiol (17aE2), a less feminizing isomer of 17β-estradiol, on longevity are restricted to males [28]. Likewise, acarbose extends the mouse lifespan to a much greater degree in males than in females [29]. We have also reported that CR responses in mice may vary from lifespan extension to no effect on survival depending not only on CR level and strain but also on sex, while the onset and impact of diseases are consistently delayed independently of these factors [30]. In addition, we have identified the preservation of an optimal amount of fat mass with age, NAD^+ levels, and the maintenance of mitochondrial function as the main predictors of improved longevity in CR mice regardless sex [30].

In accordance with these antecedents, we aimed to elucidate the impact of sex on metabolic and behavioral responses in young (3mo-old) males and females of WT or TG genotype, and to study NAD^+ and NADH levels, as well as key markers related with mitochondrial function and ultrastructure in skeletal muscle. We focused our work on this tissue because skeletal muscle is a major contributor to whole animal energy expenditure and a primary tissue responsible for glucose disposal and oxidative metabolism [31]. Skeletal muscle is also a suitable model to study potentially dimorphic mechanisms since major differences also exist between female and male skeletal muscles, including differences in energy metabolism, fiber type composition, and contractile speed, with male muscles being generally faster and having higher maximum power output than female muscles. On the contrary, female muscles are generally more resistant to fatigue, recover faster, and show less mechanical damage after exercise [32]. In addition, skeletal muscle fibres can be specially affected by aging-associated mitochondrial dysfunction leading to sarcopenia, whose onset is related with a decrease in mitochondrial content and functionality [33].

Skeletal muscle is also a site where ectopic CYB5R3 can be efficiently overexpressed [13] thus constituting an excellent model to investigate cell-autonomous mechanisms by which CYB5R3 upregulation can optimize metabolism. Moreover, CYB5R3 plays key metabolic roles in muscle cells. In vascular smooth muscle cells, CYB5R3 is critical for NO-stimulated cGMP production and vasodilation due to its ability to reduce ferric iron in soluble guanylate cyclase (sGC) heme that has been oxidized by reactive oxygen species, thus recycling its NO-sensitive form [6], preserving cardiac and vascular function under chronic hypoxic stress [34]. Moreover, CYB5R3 deficiency accelerates pulmonary hypertension development in sickle cell mice [35] and amplifies angiotensin II-induced hypertension [36]. Likewise, CYB5R3 also reduces heme iron of myoglobin facilitating oxygen binding and transport to the mitochondria in muscle fibers [1,5]. In cardiomyocytes, CYB5R3 regulates redox equilibrium, and its deletion causes cardiac hypertrophy, bradycardia, and sudden cardiac death in male mice, but not in females [37]. Thus, identification of prominent pathways regulated by CYB5R3 overexpression in skeletal muscle is relevant to understand the mechanisms associated with the effects of CYB5R3 on longevity in both sexes.

Our previous research carried out with male mice has demonstrated the existence of a relationship between CYB5R3 overexpression and the control of fat mass because 9-10 mo-old TG males exhibited an increase of fat mass without changing body weight in comparison with age-matched WT controls [11]. The results we report here for younger (3 mo) mice have revealed the differences in body weight and body composition expected to occur between males and females (*i.e.* higher

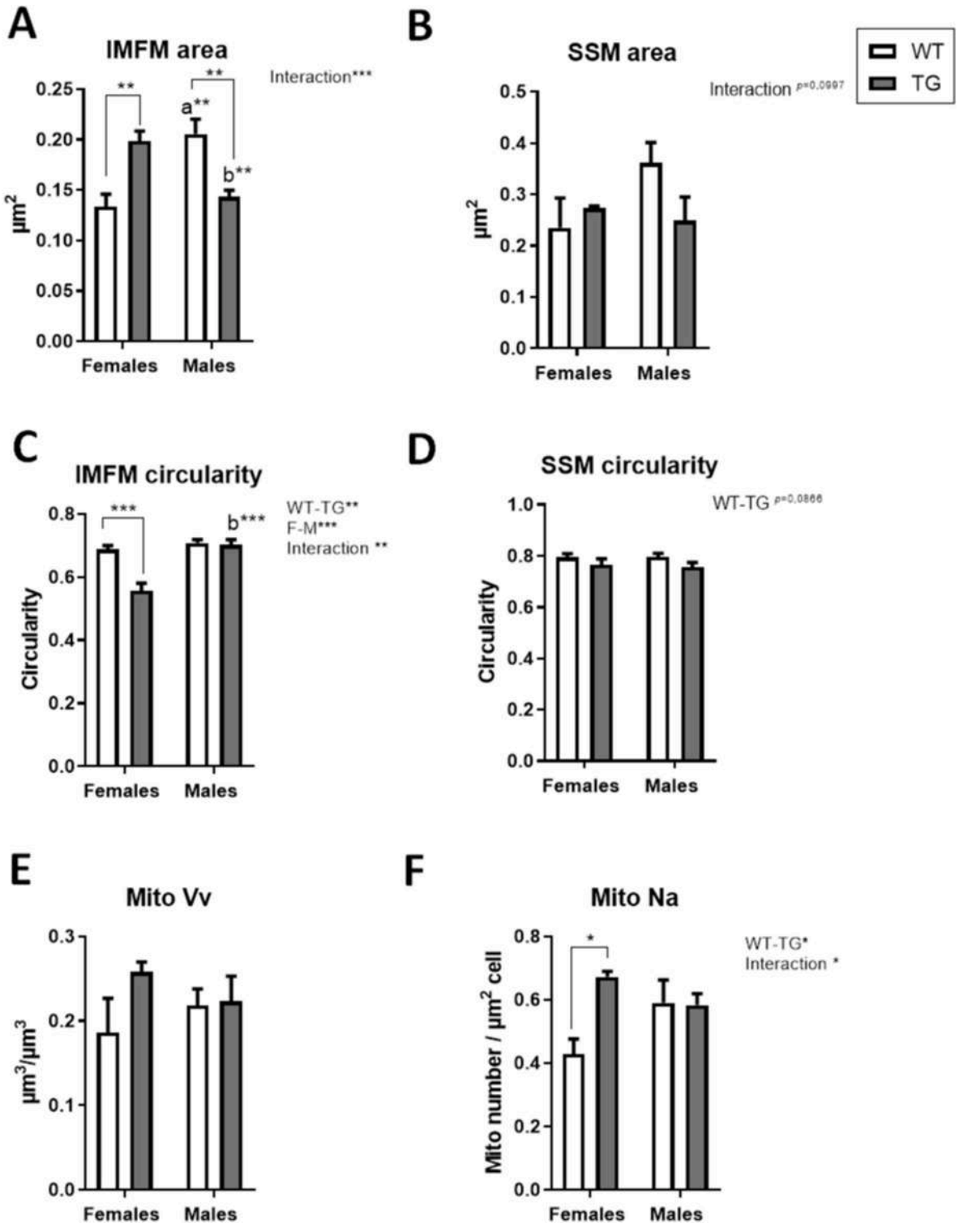

Fig. 10. Planimetric and morphometric features of red fibers mitochondria in cross-sections of red gastrocnemius from female and male mice of WT and TG genotypes. Panels show Intermyofibrillar mitochondria (IMFM) area (A), subsarcolemmal mitochondria (SSM) area (B), IMFM circularity (C), SSM circularity (D), volume density (Vv) and numerical profile density (Na) (F). Asterisks in the bars denote the level of significance of the differences between genotypes (WT *vs*. TG) for a given sex, whereas a trend is denoted by *p* value. Asterisks that are accompanied by "a" (for WT) or "b" (for TG) denote significant differences between females and males for a given genotype. Global effects of sex (regardless of genotype) are represented as "F-M" with asterisks, while overall effects of genotype (regardless of sex) are represented as "WT-TG" with asterisks. The interaction "sex x genotype" is also indicated when appropriate. Data are shown as means ± SEM of 4 animals per group. Global effects of age or genotype were evaluated by two-way ANOVA. Means were compared by Student's *t*-test, whereas those in panels C and D were compared by Mann–Whitney nonparametric test.

weight, lean mass, and lean-to-fat ratio in the males) but no differences in these parameters due to CYB5R3 overexpression were observed for any sex. One possible explanation for the apparent discrepancy between our previous findings and the results we show here is that the effects of CYB5R3 overexpression on body composition are manifested later in life. In addition, since we fed mice with a standard rodent chow diet whereas Martín-Montalvo et al. [11] fed mice with AIN93G diet, it is also possible that diet composition is a key factor that determines the outcome of CYB5R3 overexpression in the regulation of body composition. We have also reported that CYB5R3 is a key determinant in the control of organ and body weight with CR because CYB5R3 overexpression led to a greater preservation of body and liver weight in 7mo-old males fed a CR diet based on the AIN93 M formulation [24].

We previously showed that carbon metabolism is a prominent target of CYB5R3 overexpression since 9 to 10mo-old TG males that had been fed for 16 weeks on a AIN93G diet, consumed less oxygen per gram of body weight and preferentially used carbohydrates to meet their energy needs, as indicated from their increased RER [11]. However, 3mo-old mice of TG or WT genotype did not exhibit these striking differences in RER, as we only evidenced higher RER in TGF during the light period of the first feeding cycle. Moreover, no statistically significant differences among genotypes were found in males throughout the whole feeding-fasting-refeeding cycle, and we even evidenced a trend towards decreased RER in TGM compared with WTM during some periods of the feeding-fast-refeeding cycle. Again, the possibility exists that CYB5R3-induced adaptations of carbon metabolism are also manifested later in life, particularly in the males, and may be affected by diet composition as well. In any case, elevated respiration with higher O_2 consumption and CO_2 release in females is consistent with the fact that smaller animals (e.g., female compared to male mice) have higher energy expenditure, as previously reported for C57BL/6 mice [38]. However, we did not find statistically significant differences in spontaneous ambulatory activity over the course of the fed-fasted–refed cycle between males and females.

We previously showed that overexpressed CYB5R3 is efficiently targeted to skeletal muscle mitochondria in TG males regardless age [13]. However, it is unknown if ectopically expressed CYB5R3 is targeted to extramitochondrial membranes, which are also sites containing the endogenous reductase [1]. Moreover, since our previous study was carried out exclusively with males, it remains to be determined if the CYB5R3 overexpression pattern in skeletal muscle from TG mice is dependent on sex. Despite the higher abundance of endogenous CYB5R3 in WT females, the transgene was equally overexpressed in skeletal muscle and efficiently targeted to a membranous fraction enriched in mitochondria both in TGM and TGF, which agrees with our previous work developed in males [13,24]. It remains for further research to investigate if this overexpression pattern is maintained along aging in TGF, as we have already demonstrated for TGM [13]. Nevertheless, we show here for the first time that ectopically expressed CYB5R3 is also accumulated efficiently in a fraction enriched in microsomes and plasma membrane-derived vesicles. Since these high-speed precipitates gave the lowest signal for the OMM marker VDAC, it is not expected that cross-contamination with fragments derived from the OMM is the main factor accounting for the presence of ectopic CYB5R3 in this fraction, although some contribution cannot be completely ruled out given the substantial accrual of ectopic CYB5R3 in skeletal muscle mitochondria from TG mice. Enrichment of CYB5R3 in skeletal muscle microsomes and plasma membranes from TG mice opens novel perspectives into the role of CYB5R3 overexpression in the regulation of processes linked to these membranes that may play key roles in healthspan and lifespan, as the various biosynthetic and metabolic pathways in which CYB5R3 participates at the endoplasmic reticulum and the plasma membrane (see Introduction). Since CYB5R3 is synthesized by cytosolic ribosomes and then post-translationally inserted into the cytosolic side of membranes after its N-terminal myristoylation [1], the lack of a significant CYB5R3 polypeptide signal in cytosolic high-speed supernatants obtained from WT or TG mice indicates that CYB5R3 (either endogenous or overexpressed) is efficiently processed and inserted into phospholipid bilayers as an integral membrane protein.

NADH and NAD^+ are substrates for a plethora of redox enzymes using these compounds as electron donor or acceptor respectively, and the NAD^+/NADH ratio is a key regulator of the balance between oxidative and reductive reactions [39]. Moreover, NAD^+ is strongly related with the prevention of metabolic diseases and the promotion of healthy aging, mostly due to its role as cofactor for SIRTs [40,41]. To this sense, the salutary effects of CYB5R3 overexpression might be partly mediated by the enhanced oxidation of NADH to NAD^+, and we previously reported a trend towards higher NAD^+/NADH ratio in liver from male mice overexpressing CYB5R3 [11]. In skeletal muscle, we have found that NAD^+ and NADH levels (as measured on a protein basis) were higher in females than in males. Frederic et al. [42] showed that NAD^+ concentrations in the mixed hindlimb muscles (quadriceps, gastrocnemius, and tibialis anterior) were similar in male and female mice. However, these measurements were given on a muscle weight basis, and it is even unclear whether wet or dry muscle weight was used to normalize NAD^+ concentration [43], which precludes a direct comparison of these data with our results. CYB5R3 overexpression significantly elevated NADH in both sexes, although differences were not statistically significant for NAD^+. Nevertheless, the pattern of NAD^+ changes closely resembled that of NADH, and no differences in the NAD^+/NADH ratio were observed between any of the experimental groups. This agrees with the previous demonstration that skeletal muscle-specific overexpression of nicotinamide phosphoribosyltransferase (NAMPT), a rate limiting enzyme in salvage NAD^+ biosynthesis, equally elevated NAD^+ and NADH in this tissue, suggesting the existence of equilibration mechanisms between these two redox forms to maintain the NAD^+/NADH ratio across a homeostatic range of absolute concentrations. Moreover, it remains unresolved whether changes in absolute NAD^+ concentration or in the redox ratio play a greater role in mediating the effects of NAD^+-boosting interventions [44].

Since the upregulation of CYB5R3 is known to enhance aerobic respiration in cellular systems [45], we next studied how several markers related with mitochondrial biogenesis, dynamics and oxidative capacity were regulated in skeletal muscle by CYB5R3 overexpression in both males and females. Overall, the abundance of selected markers of mitochondrial complexes, particularly complex IV, was higher in males than in females, and CYB5R3 overexpression further increased abundance of complex I and III markers in males. We previously reported that CYB5R3 overexpression by itself increased the levels of mitochondrial complexes in skeletal muscle from 7mo-old males that had been fed *ad libitum* for 4 months with AIN93 M diet. Although CR also produced a generalized increase in the levels of mitochondrial complexes, this effect was blunted when CR was combined with CYB5R3 overexpression [24]. Apart from a trend towards an increase in complex II, CYB5R3 did not produce major changes in the abundance of mitochondrial complexes markers in females, but it did upregulate cytochrome *c*, proposed as an indicator of mitochondrial density in murine skeletal muscle [46].

Despite the higher abundance of mitochondrial complexes markers in males, we did not find differences in maximal oxygen consumption between males and females. Since the assay for measuring oxygen consumption in mitochondria isolated from frozen tissue relies on the preservation of functional supercomplexes [17], our results suggest that supercomplexes formation is optimized in females. Interestingly, a lower abundance of free catalytic complex I components improves complex I assembly, leading to higher efficacy of substrate utilization and oxygen consumption rates with decreased superoxide production, and enabling enhanced longevity [47]. Of note, CYB5R3 overexpression augmented maximal complex IV-linked oxygen consumption specifically in females, without increasing the abundance of mitochondrial complexes markers.

Mitochondrial homeostasis relies on the biogenesis of new constituents, as well as on repeated fusion and fission cycles which intermix these constituents and on mitophagy which is linked to mitochondrial

fission [48]. The maintenance of these processes is particularly needed to preserve health of long-lived postmitotic cells as skeletal muscle fibers, in contrast to mitotic cells that can rely on apoptosis as a quality control mechanism [31]. Our results support that the dynamic behaviour of skeletal muscle mitochondria may be enhanced in females, and especially in those overexpressing CYB5R3 because both MFN-1 and FIS-1 were found increased in females in comparison with males, and DRP-1 was significantly upregulated by CYB5R3 overexpression in females but not in males. Moreover, consistent with the selective increase of DRP-1 by CYB5R3 overexpression in females, we also evidenced a concerted upregulation of key markers of mitochondrial biogenesis (TFAM and NRF1), mitophagy (PARKIN) and oxidative metabolism (cleaved SIRT3) in the same group, indicating the existence of a higher mitochondrial turnover in TGF. The increase of DRP-1 in skeletal muscle from TGF is noteworthy because the loss of mitochondrial fission in satellite cells due to aging or to genetic ablation of DRP-1 deregulates the mitochondrial electron transport chain, leading to inefficient oxidative metabolism and mitophagy and increased oxidative stress, which impairs regenerative competence throughout adult life, while these defects can be rescued by the re-establishment of mitochondrial dynamics, either by activating fission or by preventing fusion [49]. It is tempting to speculate that CYB5R3 overexpression might preserve regenerative capacity of skeletal muscle with aging. Testing of this interesting hypothesis remains for further research.

Elevations of SIRT3, PGC-1α, and cytochrome *c* have been also found in a long-lived rat strain that was selectively bred for high intrinsic aerobic exercise capacity [46,50,51]. In our model, skeletal muscle from TGF combined the increase of SIRT3 with higher levels of acetylated proteins in mitochondria. SIRT3 contributes to the regulation of mitochondrial content and substrate utilization, and fatty acid oxidation is decreased in many tissues from SIRT3 knockout mice, including skeletal muscle, allegedly because of increased acetylation of mitochondrial proteins and/or a reduced mitochondrial content. However, the notion that lysine acetylation causes broad-ranging damage to mitochondrial quality and performance has been recently challenged after the recent demonstration that the functional phenotype of hyperacetylated mitochondria in a double-knockout mouse model with a genetic ablation of both carnitine acetyltransferase and SIRT3 is largely normal, indicating that redox balance and carbon flux are modulated by the acetyl-lysine turnover rather than by acetyl-lysine stoichiometry [52]. Increases of several markers of mitochondrial biogenesis and function as well as maximal respiration rates in skeletal muscle from TGF are consistent with this idea.

Alterations in mitochondrial function in different settings, as aging, exercise, and CR are also linked to changes of mitochondrial size and shape [53]. Thus, we carried out a study by transmission electron microscopy to confirm whether the observed alterations in mitochondrial biochemical parameters were also translated into ultrastructural modifications. While we found no changes in SSM, the size of IMM was increased by CYB5R3 overexpression in females but decreased in males. Circularity of IMFM was also decreased by CYB5R3 overexpression in females but unchanged in males. The quantitative parameter Na, a marker of numerical abundance of the organelle, was significantly increased in TG females but not in males. Taken together the biochemical and structural data, our results fit with a scenario where augmented mitochondrial fission is coupled with the upregulation of mitochondrial biogenesis and clearance of smaller mitochondrial profiles by mitophagy in females overexpressing CYB5R3.

Whereas CYB5R3 upregulation stimulates aerobic respiration (see above), CYB5R3 loss in cardiac muscle causes hypoxia, which has been attributed to oxidation of heme in myoglobin, and this could affect oxygen supply to the mitochondrial electron transport chain [1,5,6]. Thus, alterations of hypoxia-related signaling could explain, at least partially, some of the metabolic and mitochondrial changes observed in TG mice. In contrast with other tissues, skeletal muscle expresses high amounts of HIF1 in normoxia, although it levels can be further increased in hypoxia [54]. Although we cannot exclude the participation of HIF1 in determining the phenotype of TG females we show here, at least partially, it is unlikely that this pathway plays a major role because HIF1 abundance was unchanged for all our experimental groups. Despite this lack of changes in HIF-1, we found that that HO-1, a downstream target of HIF-1 signaling [55], was increased in males compared with females regardless genotype and, importantly, it was dramatically upregulated by CYB5R3 overexpression in males but not in females. Expression of HO-1 can be also activated under oxidative stress conditions through a pathway controlled by the antioxidant transcription factor Nrf-2 in many tissues, including skeletal muscle [56]. A lack of HO-1 upregulation in skeletal muscles from TG females is thus noteworthy as it is supportive that the increase of oxygen consumption shown in mitochondria from females overexpressing CYB5R3 is not accompanied with higher rates of oxidative stress.

Of note, the dimorphic pattern of skeletal muscle adaptations we show here for TG mice agrees with the main findings encountered in several models involving alterations in signalling by estrogens, which are involved in the maintenance of muscle function, and their insufficiency affects muscle strength and regeneration in females [57]. Reduced estrogen receptor α (ERα) expression in skeletal muscle is associated with glucose intolerance and adiposity both in women and in female mice, and these disturbances can be recapitulated in muscle-specific ERα knockout mice, which is paralleled by diminished muscle oxidative metabolism, aberrant mitochondrial morphology, overproduction of reactive oxygen species, and impairment in basal and stress-induced mitochondrial fission dynamics driven by imbalanced signalling through DRP1, and defective mitophagy characterized by decreased levels of PINK1 and PARKIN [31]. However, skeletal muscles of ER-deficient males combined the advantages of male and female muscles since they performed better during fatigue and recovery but were still as fast [32]. In accordance with these dimorphic effects of estrogens in males and in females, estrogen administration increased superoxide production in male Fischer 344 rats [58], which is opposite to a lowering effect on reactive oxygen species production in females [20]. In a muscle-specific ERβ-knockout mouse model it was found that young females displayed a decrease in the mass of fast muscles, and in a satellite cell-specific ERβ-knockout mouse model females, but not males, exhibited impaired muscle regeneration following acute muscle injury, which was explained based on reduced proliferation and increased apoptosis of satellite cells [57]. The dimorphic pattern of HO-1 upregulation with CYB5R3 overexpression we have shown here is also consistent with these findings. Interestingly, CYB5R3 is a co-factor of steroid biosynthesis pathways, and the two isoforms of cytochrome b_5 (CYB5A and CYB5B) are also allosteric effectors that interact with the cytochrome P450c17 oxidoreductase complex to stimulate 17,20-lyase activity in the biosynthetic pathway of sex hormones [59,60]. It remains for further investigation to elucidate if changes of estrogenic signalling related with alterations in hormone biosynthesis rates are mechanistically linked with the physiological effects of CYB5R3 overexpression in skeletal muscle.

In summary, our results have demonstrated the existence of adaptations to modulate mitochondrial biogenesis, fusion/fission dynamics and oxidative capacity in skeletal muscle from mice overexpressing CYB5R3, these processes being upregulated particularly in females. CYB5R3-overexpressing TG mice constitute a valuable tool for the investigation of sexually dimorphic, and potentially novel, mechanisms of aging.

Sources of funding

Work in JMV laboratory was supported by the Spanish Ministerio de Ciencia, Innovación y Universidades (MCIU)/Agencia Estatal de Investigación (AEI) grant RTI2018-100695-B-I00, PID2021-126280OB-I00, Spanish Junta de Andalucía grants P18-RT-4264, 1263735-R and BIO-276, the Fondo Europeo de Desarrollo Regional (FEDER) from the

European Union, and Universidad de Córdoba. LMSM and SRL held FPI predoctoral contracts funded by MINECO (references PRE2019-087,438 and BES-2016-078,229, respectively). RdC is supported by the Intramural Research Program of the National Institute on Aging of the National Institutes of Health.

Compliance with ethical standards

All animals were cared for in accordance with the University of Córdoba policy for animal welfare, which complies current European, Spanish and Andalusian regulations and is in accordance with the Guide for the Care and Use of Laboratory Animals published by the US National Institutes of Health and the 1964 Declaration of Helsinki and its later amendments. This study was approved by the bioethics committee of the University of Córdoba and authorized by the Consejería de Agricultura, Pesca y Desarrollo Rural, Junta de Andalucía (authorization code: 8/03/2019/029).

Authors' contributions

JMV and RdC conceived and designed the project; RdC developed the transgenic line of CYB5R3-overexpressing mice; SRL and LMSM were responsible of raising, maintaining, and genotyping the colony of mice; LMSM, CPS, JAGR and MIB performed the experimental determinations and conducted the data analysis; LMSM, JAGR and MIB carried out ultrastructural analyses; JAGR, MIB, CLP and RdC provided valuable advice; JMV and RdC provided the resources and the funding. JMV and LMSM wrote the original manuscript draft; all authors edited and reviewed the manuscript.

Data availability statement

The data that support the findings of this study are available from the corresponding author upon reasonable request.

Declaration of competing interest

Luz Marina Sánchez-Mendoza, Carlos Pérez-Sánchez, Sandra Rodríguez-López, Chary López-Pedrera, Miguel Calvo-Rubio, Rafael de Cabo, María I. Burón, José A. González-Reyes, and José M. Villalba declare that they have no competing interests.

Acknowledgements

Authors are indebted to the personnel of the Servicio Centralizado de Apoyo a la Investigación (SCAI; University of Córdoba) for technical support with the transmission electron microscope, and to the personnel of the Servicio de Animales de Experimentación (SAEX; Universidad de Córdoba) for their technical support in the maintenance of the mouse colony and in procedures with experimental animals. Funding for open access charge: Universidad de Córdoba / CBUA.

Appendix A. Supplementary data

Supplementary data to this article can be found online at https://doi.org/10.1016/j.freeradbiomed.2023.07.012.

References

[1] R. Hall, et al., Cytochrome b5 reductases: redox regulators of cell homeostasis, J. Biol. Chem. 298 (12) (2022) 15.
[2] N. Oshino, Y. Imai, R. Sato, Function of cytochrome-B5 in fatty acid desaturation by rat liver microsomes, J. Biochem. 69 (1) (1971) 155–+.
[3] V.V.R. Reddy, E. Caspi, Mechanism of C-5(6) double-bond introduction in biosynthesis of cholesterol by rat-liver microsomes - consideration of a mechanism similar to oxidation of ortho-diphenols, Eur. J. Biochem. 69 (2) (1976) 577–582.
[4] J.C. Sacco, L.A. Trepanier, Cytochrome b(5) and NADH cytochrome b(5) reductase: genotype-phenotype correlations for hydroxylamine reduction, Pharmacogenetics Genom. 20 (1) (2010) 26–37.
[5] J.B. Wittenberg, MYOGLOBIN-FACILITATED oxygen diffusion - role of myoglobin in oxygen entry into muscle, Physiol. Rev. 50 (4) (1970) 559–+.
[6] M.M. Rahaman, et al., Cytochrome b5 reductase 3 modulates soluble guanylate cyclase redox state and cGMP signaling, Circ. Res. 121 (2) (2017) 137–+.
[7] F. Navarro, et al., Vitamin E and selenium deficiency induces expression of the ubiquinone-dependent antioxidant system at the plasma membrane, Faseb. J. 12 (15) (1998) 1665–1673.
[8] P. Navas, J.M. Villalba, R. de Cabo, Importance of plasma membrane coenzyme Q in aging and stress responses, Mitochondrion 7 (2007) S34–S40.
[9] R. De Cabo, et al., Calorie restriction attenuates age-related alterations in the plasma membrane antioxidant system in rat liver, Exp. Gerontol. 39 (3) (2004) 297–304.
[10] R. de Cabo, et al., CYB5R3: a key player in aerobic metabolism and aging? Aging-Us 2 (1) (2010) 63–68.
[11] A. Martin-Montalvo, et al., Cytochrome b(5) reductase and the control of lipid metabolism and healthspan, Npj Aging and Mechanisms of Disease 2 (2016) 12.
[12] M. Zampino, et al., Greater skeletal muscle oxidative capacity is associated with higher resting metabolic rate: results from the baltimore longitudinal study of aging, Journals of Gerontology Series a-Biological Sciences and Medical Sciences 75 (12) (2020) 2262–2268.
[13] S. Lopez-Bellon, et al., CYB5R3 overexpression preserves skeletal muscle mitochondria and autophagic signaling in aged transgenic mice, Geroscience 44 (4) (2022) 2223–2241.
[14] M. Garratt, et al., Male lifespan extension with 17-alpha estradiol is linked to a sex-specific metabolomic response modulated by gonadal hormones in mice, Aging Cell 17 (4) (2018) 14.
[15] M.F. Belcourt, et al., The intracellular location of NADH : cytochrome b(5) reductase modulates the cytotoxicity of the mitomycins to Chinese hamster ovary cells, J. Biol. Chem. 273 (15) (1998) 8875–8881.
[16] C.M. Stoscheck, Quantitation of protein, Methods Enzymol. 182 (1990) 50–68.
[17] C. Osto, et al., Measuring mitochondrial respiration in previously frozen biological samples, Curr Protoc Cell Biol 89 (1) (2020) e116.
[18] E. Gutierrez-Casado, et al., The impact of aging, calorie restriction and dietary fat on autophagy markers and mitochondrial ultrastructure and dynamics in mouse skeletal muscle, Journals of Gerontology Series a-Biological Sciences and Medical Sciences 74 (6) (2019) 760–769.
[19] E.R. Weibel, Stereological methods in cell biology - where are we - where are we going, J. Histochem. Cytochem. 29 (9) (1981) 1043–1052.
[20] A. Sanz, et al., Evaluation of sex differences on mitochondrial bioenergetics and apoptosis in mice, Exp. Gerontol. 42 (3) (2007) 173–182.
[21] B.J. Gurd, et al., In mammalian muscle, SIRT3 is present in mitochondria and not in the nucleus; and SIRT3 is upregulated by chronic muscle contraction in an adenosine monophosphate-activated protein kinase-independent manner, Metab., Clin. Exp. 61 (5) (2012) 733–741.
[22] M.B. Scher, A. Vaquero, D. Reinberg, SirT3 is a nuclear NAD(+)-dependent histone deacetylase that translocates to the mitochondria upon cellular stress, Gene Dev. 21 (8) (2007) 920–928.
[23] N.L. Price, et al., SIRT1 is required for AMPK activation and the beneficial effects of resveratrol on mitochondrial function, Cell Metabol. 15 (5) (2012) 675–690.
[24] S. Rodriguez-Lopez, et al., Mitochondrial adaptations in liver and skeletal muscle to pro-longevity nutritional and genetic interventions: the crosstalk between calorie restriction and CYB5R3 overexpression in transgenic mice, Geroscience 42 (3) (2020) 977, 994.
[25] D.E. Harrison, et al., Rapamycin fed late in life extends lifespan in genetically heterogeneous mice, Nature 460 (7253) (2009) 392. U108.
[26] R.A. Miller, et al., Rapamycin, but not resveratrol or simvastatin, extends life span of genetically heterogeneous mice, Journals of Gerontology Series a-Biological Sciences and Medical Sciences 66 (2) (2011) 191–201.
[27] R.A. Miller, et al., Rapamycin-mediated lifespan increase in mice is dose and sex dependent and metabolically distinct from dietary restriction, Aging Cell 13 (3) (2014) 468–477.
[28] D.E. Harrison, et al., 17-a-estradiol late in life extends lifespan in aging UM-HET3 male mice; nicotinamide riboside and three other drugs do not affect lifespan in either sex, Aging Cell 20 (5) (2021) 10.
[29] D.E. Harrison, et al., Acarbose, 17-alpha-estradiol, and nordihydroguaiaretic acid extend mouse lifespan preferentially in males, Aging Cell 13 (2) (2014) 273–282.
[30] S.J. Mitchell, et al., Effects of sex, strain, and energy intake on hallmarks of aging in mice, Cell Metabol. 23 (6) (2016) 1093–1112.
[31] V. Ribas, et al., Skeletal muscle action of estrogen receptor a is critical for the maintenance of mitochondrial function and metabolic homeostasis in females, Sci. Transl. Med. 8 (334) (2016) 21.
[32] B. Glenmark, et al., Difference in skeletal muscle function in males vs. females: role of estrogen receptor-beta, Am. J. Physiol. Endocrinol. Metabol. 287 (6) (2004) E1125–E1131.
[33] D.C. Wallace, A mitochondrial paradigm of metabolic and degenerative diseases, aging, and cancer: a dawn for evolutionary medicine, in: Annual Review of Genetics, Annual Reviews, Palo Alto, 2005, pp. 359–407.
[34] B.G. Durgin, et al., Smooth muscle cell CYB5R3 preserves cardiac and vascular function under chronic hypoxic stress, J. Mol. Cell. Cardiol. 162 (2022) 72–80.
[35] K.C. Wood, et al., Smooth muscle cytochrome b5 reductase 3 deficiency accelerates pulmonary hypertension development in sickle cell mice, Blood Advances 3 (23) (2019) 4104–4116.

[36] B.G. Durgin, et al., Loss of smooth muscle CYB5R3 amplifies angiotensin II-induced hypertension by increasing sGC heme oxidation, Jci Insight 4 (19) (2019) 15.
[37] N.T. Carew, et al., Loss of cardiomyocyte CYB5R3 impairs redox equilibrium and causes sudden cardiac death, J. Clin. Invest. 132 (18) (2022).
[38] Y. Adamovich, et al., Oxygen and carbon Dioxide rhythms are circadian clock controlled and differentially directed by behavioral signals, Cell Metabol. 29 (5) (2019) 1092–+.
[39] W.S. Xiao, et al., NAD(H) and NADP(H) redox couples and cellular energy metabolism, Antioxidants Redox Signal. 28 (3) (2018) 251–272.
[40] S. Imai, L. Guarente, NAD(+) and sirtuins in aging and disease, Trends Cell Biol. 24 (8) (2014) 464–471.
[41] S. Imai, L. Guarente, It takes two to tango: NAD(+) and sirtuins in aging/longevity control, Npj Aging and Mechanisms of Disease 2 (2016) 6.
[42] D.W. Frederick, et al., Loss of NAD homeostasis leads to progressive and reversible degeneration of skeletal muscle, Cell Metabol. 24 (2) (2016) 269–282.
[43] L.L. Ji, D.W. Yeo, Maintenance of NAD plus homeostasis in skeletal muscle during aging and exercise, Cells 11 (4) (2022) 25.
[44] D.W. Frederick, et al., Increasing NAD synthesis in muscle via nicotinamide phosphoribosyltransferase is not sufficient to promote oxidative metabolism, J. Biol. Chem. 290 (3) (2015) 1546–1558.
[45] E. Siendones, et al., Membrane-bound CYB5R3 is a common effector of nutritional and oxidative stress response through FOXO3a and Nrf2, Antioxidants Redox Signal. 21 (12) (2014) 1708–1725.
[46] S. Karvinen, et al., Effects of intrinsic aerobic capacity, aging and voluntary running on skeletal muscle sirtuins and heat shock proteins, Exp. Gerontol. 79 (2016) 46–54.
[47] S. Miwa, et al., Low abundance of the matrix arm of complex I in mitochondria predicts longevity in mice, Nat. Commun. 5 (2014) 12.
[48] G. Twig, O.S. Shirihai, The interplay between mitochondrial dynamics and mitophagy, Antioxidants Redox Signal. 14 (10) (2011) 1939–1951.
[49] X.T. Hong, et al., Mitochondrial dynamics maintain muscle stem cell regenerative competence throughout adult life by regulating metabolism and mitophagy, Cell Stem Cell 29 (9) (2022) 1298–+.
[50] C. Handschin, B.M. Spiegelman, Peroxisome proliferator-activated receptor gamma coactivator 1 coactivators, energy hemeostasis, and metabolism, Endocr. Rev. 27 (7) (2006) 728–735.
[51] F.W. Booth, CYTOCHROME-C protein-synthesis rate in rat skeletal-muscle, J. Appl. Physiol. 71 (4) (1991) 1225–1230.
[52] A.S. Williams, et al., Disruption of acetyl-lysine turnover in muscle mitochondria promotes insulin resistance and redox stress without overt respiratory dysfunction, Cell Metabol. 31 (1) (2020) 131–+.
[53] M. Bernier, et al., Age-dependent impact of two exercise training regimens on genomic and metabolic remodeling in skeletal muscle and liver of male mice, Npj Aging 8 (1) (2022) 18.
[54] H.P. Kubis, et al., Accumulation and nuclear import of HIF1 alpha during high and low oxygen concentration in skeletal muscle cells in primary culture, Biochim. Biophys. Acta Mol. Cell Res. 1745 (2) (2005) 187–195.
[55] L.L. Dunn, et al., Hmox1 (heme oxygenase-1) protects against ischemia-mediated injury via stabilization of HIF-1 alpha (Hypoxia-Inducible factor-1 alpha), Arterioscler. Thromb. Vasc. Biol. 41 (1) (2021) 317–330.
[56] A. Loboda, J. Dulak, Nuclear factor erythroid 2-related factor 2 and its targets in skeletal muscle repair and regeneration, Antioxidants Redox Signal. 38 (7–9) (2023) 619–642.
[57] D. Seko, et al., Estrogen receptor beta controls muscle growth and regeneration in young female mice, Stem Cell Rep. 15 (3) (2020) 577–586.
[58] J.Q. Chen, et al., Increased mitochondrial superoxide production in rat liver mitochondria, rat hepatocytes, and HepG2 cells following ethinyl estradiol treatment, Toxicol. Sci. 51 (2) (1999) 224–235.
[59] A. Robic, et al., Exploration of steroidogenesis-related genes in testes, ovaries, adrenals, liver and adipose tissue in pigs, Anim. Sci. J. 87 (8) (2016) 1041–1047.
[60] A. Robic, et al., Correlation networks provide new insights into the architecture of testicular steroid pathways in pigs, Genes 12 (4) (2021) 19.